Int J Geomath
DOI 10.1007/s13137-011-0016-z

ORIGINAL PAPER

Spatiospectral concentration in the Cartesian plane

Frederik J. Simons · Dong V. Wang

Received: 23 January 2011 / Accepted: 24 March 2011

Abstract We pose and solve the analogue of Slepian's time–frequency concentration problem in the two-dimensional plane, for applications in the natural sciences. We determine an orthogonal family of strictly bandlimited functions that are optimally concentrated within a closed region of the plane, or, alternatively, of strictly spacelimited functions that are optimally concentrated in the Fourier domain. The Cartesian Slepian functions can be found by solving a Fredholm integral equation whose associated eigenvalues are a measure of the spatiospectral concentration. Both the spatial and spectral regions of concentration can, in principle, have arbitrary geometry. However, for practical applications of signal representation or spectral analysis such as exist in geophysics or astronomy, in physical space irregular shapes, and in spectral space symmetric domains will usually be preferred. When the concentration domains are circularly symmetric in both spaces, the Slepian functions are also eigenfunctions of a Sturm–Liouville operator, leading to special algorithms for this case, as is well known. Much like their one-dimensional and spherical counterparts with which we discuss them in a common framework, a basis of functions that are simultaneously spatially and spectrally localized on arbitrary Cartesian domains will be of great utility in many scientific disciplines, but especially in the geosciences.

Keywords Bandlimited function · Commuting differential operator · Concentration problem · Eigenvalue problem · Spectral analysis · Reproducing kernel · Spherical harmonics · Sturm–Liouville problem

F. J. Simons (✉) · D. V. Wang
Department of Geosciences, Princeton University, Princeton, NJ 08544, USA
e-mail: fjsimons@alum.mit.edu

Present Address:
D. V. Wang
Department of Statistics and Operations Research,
The University of North Carolina at Chapel Hill, Chapel Hill, NC 27599, USA

Published online: 19 April 2011

Mathematics Subject Classification (2000) 42B99 · 41A30 · 86-08 · 47B15 · 46E22 · 34B24 · 45B05 · 33C55

1 Introduction

The one-dimensional prolate spheroidal wave functions (pswf) have enjoyed an enduring popularity in the signal processing community ever since their introduction in the early 1960s (Landau and Pollak 1961, 1962; Slepian and Pollak 1961). Indeed, in many scientific and engineering disciplines the pswf and their relatives the discrete prolate spheroidal sequences (dpss; Grünbaum 1981; Slepian 1978) have by now become the preferred data windows to regularize the quadratic inverse problem of power spectral estimation from time-series observations of finite extent (Percival and Walden 1993). At the deliberate cost of introducing spectral bias, windowing the data with a set of such orthogonal "tapers" lowers the variance of the "multitaper" average (Thomson 1982), which results in estimates of the power spectral density that are low-error in the mean-squared sense (Thomson 1990). As a basis for function representation, approximation and interpolation (Delsarte et al. 1985; Moore and Cada 2004; Shkolnisky et al. 2006; Xiao et al. 2001), or in stochastic linear inverse problems (Bertero et al. 1985a,b; de Villiers et al. 2001; Wingham 1992), the pswf have been less in the public eye, especially compared to wavelet analysis (Daubechies 1992; Percival and Walden 2006), though, due to advances in computation, there has been a resurgent interest in recent years (Beylkin and Monzón 2002; Karoui and Moumni 2008; Khare and George 2003; Walter and Soleski 2005), in particular as relates to using them for the numerical solution of partial differential equations (Beylkin and Sandberg 2005; Boyd 2003, 2004; Chen et al. 2005).

The pswf are the solutions to what has come to be known as "the concentration problem" (Flandrin 1998; Percival and Walden 1993) of Slepian, Landau and Pollak, in which the energy of a bandlimited function is maximized by quadratic optimization inside a certain interval of time. Vice versa, it refers to the maximization of the spectral localization of a timelimited function inside a certain target bandwidth (Slepian 1983). In the first version of the problem, the bandlimited, time-concentrated pswf form an orthogonal basis for the entire space of bandlimited signals that is also orthogonal over the particular time interval of interest. In the second version the timelimited, band-concentrated pswf are a basis for square-integrable broadband signals that are exactly confined to the interval (Landau and Pollak 1961; Slepian and Pollak 1961). In general we shall refer to all singular functions of time-bandwidth or space-bandwidth projection operators as "Slepian functions".

The fixed prescription of the "region of interest" in physical or spectral space is a deliberately narrow point of view that is well suited to scientific or engineering studies where the assumption of stationarity, prior information, or the availability of data will dictate the interval of study from the outset. This distinguishes the Slepian functions philosophically from the eigenfunctions of full-phase-space localization operators (Daubechies 1988; Simons et al. 2003) or wavelets (Daubechies and Paul 1988; Olhede and Walden 2002), with which they nevertheless share strong connections (Lilly and Park 1995; Shepp and Zhang 2000; Walter and Shen 2004, 2005). Strict localization of this type remained the driving force behind the development of Slepian

functions over fixed geographical domains on the surface of the sphere (Albertella et al. 1999; Miranian 2004; Simons et al. 2006)—which have numerous applications in geodesy (Albertella and Sacerdote 2001; Han et al. 2008a; Simons and Dahlen 2006), geomagnetism (Simons et al. 2009; Schott and Thébault 2011), geophysics (Han and Ditmar 2007; Han et al. 2008b; Han and Simons 2008; Harig et al. 2010), biomedical (Maniar and Mitra 2005; Mitra and Maniar 2006) and planetary (Evans et al. 2010; Han 2008; Han et al. 2009; Wieczorek and Simons 2005) science, and cosmology (Dahlen and Simons 2008; Wieczorek and Simons 2007)—as opposed to approaches using spherical wavelets (Chambodut et al. 2005; Faÿ et al. 2008; Fengler et al. 2007; Freeden and Windheuser 1997; Holschneider et al. 2003; Kido et al. 2003; McEwen et al. 2007; Panet et al. 2006; Schmidt et al. 2006), needlets (Marinucci et al. 2008), splines (Amirbekyan et al. 2008; Lai et al. 2009; Michel and Wolf 2008), radial basis functions (Freeden and Michel 1999; Schmidt et al. 2007), coherent states (Hall and Mitchell 2002; Kowalski and Rembieliński 2000; Tegmark 1995, 1996), or other constructions (Simons et al. 1997), which have all come of age in these fields also. Finally, we note that the very choice of the criterion to define localization is open to discussion (Narcowich and Ward 1996; Parks and Shenoy 1990; Riedel and Sidorenko 1995; Saito 2007; Wei et al. 2010); in particular, it need not necessarily include only quadratic forms (Donoho and Stark 1989).

In multiple Cartesian dimensions, in practice: in the plane, the space–frequency localization problem has received remarkably little attention beyond the initial treatment by Slepian himself (Slepian 1964), who restricted his attention to concentration over circular disks in space and spectral space (see also Brander and DeFacio 1986; Van De Ville et al. 2002). In this situation, as in the one-dimensional case, the concentration operator commutes with a second-order Sturm–Liouville differential operator, which greatly facilitates the (numerical) analysis. The scarce recent work on two-dimensional Slepian functions has focused on their being amenable to generalized Gaussian quadrature (de Villiers et al. 2003; Ma et al. 1996; Shkolnisky 2007) or on using them for multiscale out-of-sample extensions (Coifman and Lafon 2006) without straying from circular regions of interest. On square or rectangular domains Slepian functions formed by outer products of pairs of the pswf (Borcea et al. 2008; Hanssen 1997) have correspondingly square or rectangular concentration regions in spectral space, which is undesirable in geophysical applications (Simons et al. 2003).

Geographical regions are not typically squares, circles or rectangles—although usually we will require the spectral support of the Slepian functions to remain disk-like to enable isotropic feature extraction (Zhang 1994). In those studies where Cartesian domains of arbitrary geometry have been implicit or explicitly considered, as for applications in image processing (Zhou et al. 1984), radio-astronomy (Jackson et al. 1991), medical (Lindquist et al. 2006; Walter and Soleski 2008; Yang et al. 2002), radar or seismic imaging (Borcea et al. 2008) or in the specific context of multi-dimensional spectral analysis (Bronez 1988; Liu and van Veen 1992), the Slepian functions are obtained directly from the defining equation, i.e. by numerical diagonalization of the discretized space-bandwidth projection operator. This can be implemented explicitly (Percival and Walden 1993) or by iterated filtering and bounding (Jackson et al. 1991) as in the Papoulis (Kennedy et al. 2008; Papoulis 1975) or Lanczos (Golub and van Loan 1989) algorithms. Given the

characteristic step-shaped eigenvalue spectrum of the operators (Daubechies 1988, 1992; Slepian 1976, 1983) such procedures are not uniformly stable (Bell et al. 1993), and for general, non-symmetric domains, no better-behaved commuting operator exists (Brander and DeFacio 1986; Grünbaum et al. 1982; Parlett and Wu 1984). In this case we prefer the numerical solution of the Fredholm integral equation (Tricomi 1970) with which the concentration problem is equivalent, by the Nyström method (Nyström 1930), using classical Gauss–Legendre integration (Press et al. 1992). When both the spatial and spectral regions of concentration are irregular in shape and of complete generality, diagonalization of the projection operator is our only recourse.

As we have in a sense come full circle as regards "Slepian's problem", at least concerning the scalar case, and because of its deep connections within the framework of reproducing-kernel Hilbert spaces (Aronszajn 1950; Simons 2010; Yao 1967), our contribution has the character of a review. We take the reader from the beginnings of the theory in one linear dimension (Slepian and Pollak 1961) to its generalization on the surface of the unit sphere (Simons and Dahlen 2006; Simons et al. 2006), and back to the two Cartesian dimensions of the title of this paper, where, after Slepian (1964), there remained some work to be done. Our discussion is only as technical as required to make the theory available for applications in the natural sciences. Focusing on the practical and the reproducible, we are distributing all of our MATLAB computer routines freely over the World Wide Web.

2 Spatiospectral concentration on the real line

We use t to denote time or one-dimensional space and ω for angular frequency, and adopt a normalization convention (Mallat 1998) in which a real-valued time-domain signal $f(t)$ and its Fourier transform $F(\omega)$ are related by

$$f(t) = (2\pi)^{-1} \int_{-\infty}^{\infty} F(\omega) e^{i\omega t}\, d\omega, \qquad F(\omega) = \int_{-\infty}^{\infty} f(t) e^{-i\omega t}\, dt. \tag{1}$$

Following Slepian, Landau and Pollak (Landau and Pollak 1961; Slepian and Pollak 1961), the strictly bandlimited signal

$$g(t) = (2\pi)^{-1} \int_{-W}^{W} G(\omega) e^{i\omega t}\, d\omega \tag{2}$$

that is maximally concentrated within $|t| \le T$ is the one that maximizes the ratio

$$\lambda = \frac{\int_{-T}^{T} g^2(t)\, dt}{\int_{-\infty}^{\infty} g^2(t)\, dt}. \tag{3}$$

Bandlimited functions $g(t)$ satisfying problem (3) have spectra $G(\omega)$ that satisfy

$$\int_{-W}^{W} D(\omega, \omega')G(\omega')\,d\omega' = \lambda G(\omega), \quad |\omega| \le W, \tag{4a}$$

$$D(\omega, \omega') = \frac{\sin[T(\omega - \omega')]}{\pi(\omega - \omega')}. \tag{4b}$$

The corresponding time- or spatial-domain formulation is

$$\int_{-T}^{T} D(t, t')g(t')\,dt' = \lambda g(t), \quad t \in \mathbb{R}, \tag{5a}$$

$$D(t, t') = \frac{\sin[W(t - t')]}{\pi(t - t')}. \tag{5b}$$

When the pswf $g_1(t), g_2(t), \ldots$ that solve Eq. (5) are made orthonormal over $|t| \le \infty$ they are also orthogonal over the interval $|t| \le T$:

$$\int_{-\infty}^{\infty} g_\alpha g_\beta\,dt = \delta_{\alpha\beta}, \qquad \int_{-T}^{T} g_\alpha g_\beta\,dt = \lambda_\alpha \delta_{\alpha\beta}. \tag{6}$$

It now follows directly that

$$D(t, t') = \sum_{\alpha=1}^{\infty} g_\alpha(t)g_\alpha(t') \quad \text{and} \quad \sum_{\alpha=1}^{\infty} g_\alpha^2(t) = \frac{W}{\pi}. \tag{7}$$

A change of variables and a scaling transform Eq. (4) into the dimensionless eigenvalue problem

$$\int_{-1}^{1} D(x, x')\psi(x')\,dx' = \lambda\psi(x), \tag{8a}$$

$$D(x, x') = \frac{\sin[TW(x - x')]}{\pi(x - x')}. \tag{8b}$$

The eigenvalues $\lambda_1 > \lambda_2 > \cdots$ and eigenfunctions $\psi_1(x), \psi_2(x), \ldots$ depend only upon the time-bandwidth product TW. The sum of the concentration values λ relates to this as

$$N^{1D} = \sum_{\alpha=1}^{\infty} \lambda_\alpha = \int_{-1}^{1} D(x, x)\,dx = \frac{2TW}{\pi} = \frac{(2T)(2W)}{2\pi}. \tag{9}$$

The spectrum of Eq. (8) has near-unity and near-zero eigenvalues separated by a narrow transition band (Landau 1965; Slepian and Sonnenblick 1965). Thus, N^{1D}, the "Shannon number", roughly equals the number of significant eigenvalues. In other words (Landau and Pollak 1962), it is the approximate dimension of the space of signals that can be simultaneously well concentrated into finite time and frequency intervals. The eigenvalue-weighted sum of the eigenfunctions will be nearly equal to the constant in Eq. (7) over the region of concentration, as

$$\sum_{\alpha=1}^{\infty} \lambda_\alpha g_\alpha^2(t) \approx \sum_{\alpha=1}^{N^{1D}} \lambda_\alpha g_\alpha^2(t) \approx \begin{cases} N^{1D}/(2T) & \text{if } -T \le t \le T, \\ 0 & \text{otherwise.} \end{cases} \tag{10}$$

The integral operator in Eq. (8) commutes with a Sturm–Liouville differential operator (Slepian 1983; Slepian and Pollak 1961), to the effect that although $\chi \neq \lambda$, we can solve for the functions ψ also from

$$\frac{d}{dx}\left[(1-x^2)\frac{d\psi}{dx}\right] + \left[\chi - \frac{(N^{1D})^2\pi^2}{4}x^2\right]\psi = 0, \quad |x| \le 1. \tag{11}$$

At N discrete values of $x = 0, \ldots, N-1$, the eigenfunctions $\psi(x)$ of Eq. (11) can be found by diagonalization of a simple symmetric tridiagonal matrix (Grünbaum 1981; Percival and Walden 1993; Slepian 1978) with elements

$$T_{xx} = [(N-1-2x)/2]^2 \cos(2\pi W), \tag{12a}$$
$$T_{x\,x+1} = (x+1)(N-x-1)/2. \tag{12b}$$

The matching concentration eigenvalues λ can then be obtained directly from Eq. (8). Compared to those, the Sturm–Liouville eigenvalues χ are very regularly distributed and thus the computation of the Slepian functions via diagonalization of Eq. (12) is always stable (Percival and Walden 1993).

3 Spatiospectral concentration on a sphere

We use $\hat{\mathbf{r}} = (\theta, \phi)$ to denote a location at colatitude θ and longitude ϕ on the unit sphere $\Omega = \{\hat{\mathbf{r}} : \|\hat{\mathbf{r}}\| = 1\}$, and adopt a normalization convention (Dahlen and Tromp 1998; Edmonds 1996) in which a real-valued time-domain signal $f(\hat{\mathbf{r}})$ and its spherical-harmonic transform f_{lm} at degree l and order m are related by

$$f(\hat{\mathbf{r}}) = \sum_{l=0}^{\infty}\sum_{m=-l}^{l} f_{lm} Y_{lm}(\hat{\mathbf{r}}), \qquad f_{lm} = \int_\Omega f(\hat{\mathbf{r}}) Y_{lm}(\hat{\mathbf{r}})\, d\Omega. \tag{13}$$

Following Simons, Wieczorek and Dahlen (Simons et al. 2006) the strictly bandlimited signal

$$g(\hat{\mathbf{r}}) = \sum_{l=0}^{L} \sum_{m=-l}^{l} g_{lm} Y_{lm}(\hat{\mathbf{r}}) \tag{14}$$

that is maximally concentrated within a region $R \subset \Omega$ maximizes the ratio

$$\lambda = \frac{\int_R g^2(\hat{\mathbf{r}})\, d\Omega}{\int_\Omega g^2(\hat{\mathbf{r}})\, d\Omega}. \tag{15}$$

Bandlimited functions $g(\hat{\mathbf{r}})$ satisfying problem (15) have spectra g_{lm} that satisfy

$$\sum_{l'=0}^{L} \sum_{m'=-l'}^{l'} D_{lm,l'm'} g_{l'm'} = \lambda g_{lm}, \quad 0 \le l \le L, \tag{16a}$$

$$D_{lm,l'm'} = \int_R Y_{lm} Y_{l'm'}\, d\Omega. \tag{16b}$$

Through the addition theorem (Dahlen and Tromp 1998), the corresponding spatial-domain formulation is

$$\int_R D(\hat{\mathbf{r}}, \hat{\mathbf{r}}') g(\hat{\mathbf{r}}')\, d\Omega' = \lambda g(\hat{\mathbf{r}}), \quad \hat{\mathbf{r}} \in \Omega, \tag{17a}$$

$$D(\hat{\mathbf{r}}, \hat{\mathbf{r}}') = \sum_{l=0}^{L} \left(\frac{2l+1}{4\pi} \right) P_l(\hat{\mathbf{r}} \cdot \hat{\mathbf{r}}'), \tag{17b}$$

where P_l is the Legendre function. When the functions $g_1(\hat{\mathbf{r}}), g_2(\hat{\mathbf{r}}), \ldots, g_{(L+1)^2}(\hat{\mathbf{r}})$ that solve Eq. (17) are orthonormal over Ω they are also orthogonal over the region R:

$$\int_\Omega g_\alpha g_\beta\, d\Omega = \delta_{\alpha\beta}, \qquad \int_R g_\alpha g_\beta\, d\Omega = \lambda_\alpha \delta_{\alpha\beta}. \tag{18}$$

From Eqs. (17)–(18) we then immediately obtain the relations

$$D(\hat{\mathbf{r}}, \hat{\mathbf{r}}') = \sum_{\alpha=1}^{(L+1)^2} g_\alpha(\hat{\mathbf{r}}) g_\alpha(\hat{\mathbf{r}}') \quad \text{and} \quad \sum_{\alpha=1}^{(L+1)^2} g_\alpha^2(\hat{\mathbf{r}}) = \frac{(L+1)^2}{4\pi}. \tag{19}$$

Asymptotically, as the spatial area $A \to 0$, and $L \to \infty$, Eq. (17) becomes (Simons and Dahlen 2007; Simons et al. 2006)

$$\int_{R_*} D(\boldsymbol{\xi}, \boldsymbol{\xi}')\psi(\boldsymbol{\xi}')\, d\Omega'_* = \lambda\psi(\boldsymbol{\xi}), \tag{20a}$$

$$D(\boldsymbol{\xi}, \boldsymbol{\xi}') = \frac{(L+1)\sqrt{A/4\pi}}{2\pi} \frac{J_1[(L+1)\sqrt{A/4\pi}\|\boldsymbol{\xi} - \boldsymbol{\xi}'\|]}{\|\boldsymbol{\xi} - \boldsymbol{\xi}'\|}, \tag{20b}$$

where the scaled region R_* now has area 4π and J_1 is the first-order Bessel function of the first kind. As in the one-dimensional case (9), the eigenvalues $\lambda_1 \geq \lambda_2 \geq \ldots$ and eigenfunctions $\psi_1(\boldsymbol{\xi}), \psi_2(\boldsymbol{\xi}), \ldots$ depend only upon the product of the maximal degree L and the area A. The sum of the concentration values λ, the space-bandwidth product or "spherical Shannon number", $N^{3\mathrm{D}}$, once again roughly the number of significant eigenvalues, is:

$$\begin{aligned} N^{3\mathrm{D}} &= \sum_{\alpha=1}^{(L+1)^2} \lambda_\alpha = \sum_{l=0}^{L} \sum_{m=-l}^{l} D_{lm,lm} = \int_R D(\hat{\mathbf{r}}, \hat{\mathbf{r}})\, d\Omega, \\ &= \int_{R_*} D(\boldsymbol{\xi}, \boldsymbol{\xi})\, d\Omega_* = (L+1)^2 \frac{A}{4\pi}. \end{aligned} \tag{21}$$

The first $N^{3\mathrm{D}}$ orthogonal eigenfunctions $g_\alpha, \alpha = 1, 2, \ldots, N^{3\mathrm{D}}$, with significant eigenvalues $\lambda_\alpha \approx 1$, provide an essentially uniform coverage of the region R, reaching the constant of Eq. (19) in the following sense:

$$\sum_{\alpha=1}^{(L+1)^2} \lambda_\alpha g_\alpha^2(\hat{\mathbf{r}}) \approx \sum_{\alpha=1}^{N^{3\mathrm{D}}} \lambda_\alpha g_\alpha^2(\hat{\mathbf{r}}) \approx \begin{cases} N^{3\mathrm{D}}/A & \text{if } \hat{\mathbf{r}} \in R, \\ 0 & \text{otherwise.} \end{cases} \tag{22}$$

Irrespectively of the particular region of concentration that they were designed for, the complete set of bandlimited spatial Slepian eigenfunctions $g_1, g_2, \ldots, g_{(L+1)^2}$ is a basis for bandlimited scalar processes anywhere on the surface of the unit sphere (Simons and Dahlen 2006; Simons et al. 2006). The reduced set $g_1, \ldots, g_{N^{3\mathrm{D}}}$, with eigenvalues $\lambda \approx 1$, is an approximate basis for bandlimited processes that are primarily localized to the region R (Simons et al. 2009). Thus $N^{3\mathrm{D}}$ is the approximate dimension of the space of signals that can be simultaneously well concentrated into finite spatial and spectral intervals on the surface of the unit sphere. Equation (20) depends only on this combination of bandwidth and spatial area, as in the one-dimensional case, Eq. (8).

When the region of concentration is a circularly symmetric cap of colatitudinal radius Θ, centered on the North Pole, the colatitudinal parts $\mathsf{g}(\theta)$ of the separable solutions to Eq. (17),

$$g(\theta,\phi)=\begin{cases}\sqrt{2}\,\mathsf{g}(\theta)\cos(m\phi) & \text{if } -L\le m<0,\\ \mathsf{g}(\theta) & \text{if } m=0,\\ \sqrt{2}\,\mathsf{g}(\theta)\sin(m\phi) & \text{if } 0<m\le L,\end{cases} \tag{23}$$

are, owing to a commutation relation (Grünbaum et al. 1982), identical to those of the Sturm–Liouville equation

$$\frac{d}{d\mu}\left[(\mu-\cos\Theta)(1-\mu^2)\frac{d\mathsf{g}}{d\mu}\right]+\left[\chi+L(L+2)\mu-\frac{m^2(\mu-\cos\Theta)}{1-\mu^2}\right]\mathsf{g}=0, \tag{24}$$

with $\mu=\cos\theta$ and $\chi\neq\lambda$. At constant m, their values g_{lm} in the expansion (14) can be found by diagonalization of a simple symmetric tridiagonal matrix (Grünbaum et al. 1982; Simons et al. 2006) with elements

$$T_{ll}=-l(l+1)\cos\Theta, \tag{25a}$$

$$T_{ll+1}=[l(l+2)-L(L+2)]\sqrt{\frac{(l+1)^2-m^2}{(2l+1)(2l+3)}}. \tag{25b}$$

When the region of concentration is a pair of axisymmetric polar caps of common radius Θ centered on the North and South Pole, the $\mathsf{g}(\theta)$ solve the Sturm–Liouville equation

$$\frac{d}{d\mu}\left[(\mu^2-\cos^2\Theta)(1-\mu^2)\frac{d\mathsf{g}}{d\mu}\right]+\left[\chi+L_p(L_p+3)\mu^2-\frac{m^2(\mu^2-\cos^2\Theta)}{1-\mu^2}\right]\mathsf{g}=0, \tag{26}$$

where $L_p=L$ or $L_p=L-1$ depending whether the order m of the functions $g(\theta,\phi)$ in Eq. (23) is odd or even, and whether the bandwidth L is odd or even (Grünbaum et al. 1982; Simons and Dahlen 2006). The expansion coefficients of the optimally concentrated antipodal polar-cap eigenfunctions require the numerical diagonalization of the symmetric tridiagonal matrix (Simons and Dahlen 2006) with elements

$$\begin{aligned}T^p_{ll}=&-l(l+1)\cos^2\Theta+\frac{2}{2l+3}[(l+1)^2-m^2]\\&+[(l-2)(l+1)-L_p(L_p+3)]\left[\frac{1}{3}-\frac{2}{3}\,\frac{3m^2-l(l+1)}{(2l+3)(2l-1)}\right],\end{aligned} \tag{27a}$$

$$T^p_{ll+2}=\frac{[l(l+3)-L_p(L_p+3)]}{2l+3}\sqrt{\frac{[(l+2)^2-m^2][(l+1)^2-m^2]}{(2l+5)(2l+1)}}. \tag{27b}$$

Every other degree in the expansion for the equatorially (anti-)symmetric double-polar cap functions is skipped (Simons and Dahlen 2006), hence the $l+2$ subscript

for the elements off the main diagonal in Eq. (27b). The concentration values λ can be determined from the defining equations (16) or (17). Compared to these, the Sturm–Liouville eigenvalues χ in Eqs. (24) and (26) are very regularly spaced, and thus the computations for these special cases are inherently stable.

4 Spatiospectral concentration in the Cartesian plane

We now turn to the multi-dimensional Cartesian case, first discussed by Slepian (1964), noting that we have set ourselves up for a result that is analogous to Eq. (20). Indeed, in the asymptotic regime of an infinitely large bandwidth and an infinitesimally small region on the surface of the unit sphere, the spherical and Cartesian concentration problems are of course equivalent (Simons and Dahlen 2007; Simons et al. 2006).

Another note concerns the equivalence between the temporal or spatial and spectral forms of the concentration problems. In writing Eqs. (4)–(5), and Eqs. (16)–(17), respectively, we have exclusively considered strictly bandlimited, time- or space-concentrated Slepian functions. Strictly time- or spacelimited, band-concentrated functions can be obtained via an appropriate restriction of the integration domains in these equations, and the resulting new functions can be obtained from the old ones by simple truncation and rescaling. Both for the one-dimensional and spherical situations this distinction is usually made more explicitly elsewhere (Landau and Pollak 1961; Simons et al. 2006; Slepian and Pollak 1961), and in what follows we once again treat both cases separately.

For applications in the geosciences, we focus on the two-dimensional, flat geometry of geographical maps: the Cartesian plane $\mathbb{R}^2$, with a spatial coordinate vector $\mathbf{x}$ and a spectral coordinate vector $\mathbf{k}$. To wit, we formulate the concentration problem as follows: in spite of the Paley-Wiener theorem, which states that functions cannot be spatially and spectrally restricted at the same time (Daubechies 1992; Mallat 1998), can we construct (real) functions that are localized to, say, the shape of Belgium, in $\mathbf{x}$-space, while having a Fourier transform localized to, say, the (Hermitian) shape of a pair of triangles, in $\mathbf{k}$-space? Yes we can!

4.1 Preliminary considerations

A real-valued, square-integrable function $f(\mathbf{x})$ defined in the plane has the two-dimensional Fourier representation

$$f(\mathbf{x}) = (2\pi)^{-2} \int_{\mathbb{R}^2} F(\mathbf{k}) e^{i\mathbf{k}\cdot\mathbf{x}} \, d\mathbf{k}, \qquad F(\mathbf{k}) = \int_{\mathbb{R}^2} f(\mathbf{x}) e^{-i\mathbf{k}\cdot\mathbf{x}} \, d\mathbf{x}, \tag{28}$$

with $F(\mathbf{k}) = F^*(-\mathbf{k})$. The Fourier orthonormality relation is

$$(2\pi)^{-2} \int_{\mathbb{R}^2} e^{i\mathbf{k}\cdot(\mathbf{x}-\mathbf{x}')} \, d\mathbf{k} = \delta(\mathbf{x}, \mathbf{x}'), \tag{29}$$

which defines the delta function in the usual distributional sense

$$\int_{\mathbb{R}^2} f(\mathbf{x}')\delta(\mathbf{x},\mathbf{x}')\,d\mathbf{x}' = f(\mathbf{x}). \tag{30}$$

Likewise, in the spectral domain we may write

$$(2\pi)^{-2}\int_{\mathbb{R}^2} e^{i(\mathbf{k}-\mathbf{k}')\cdot\mathbf{x}}\,d\mathbf{x} = \delta(\mathbf{k},\mathbf{k}'). \tag{31}$$

By Parseval's relation the energies in the spatial and spectral domains are identical:

$$\int_{\mathbb{R}^2} f^2(\mathbf{x})\,d\mathbf{x} = (2\pi)^{-2}\int_{\mathbb{R}^2} |F(\mathbf{k})|^2\,d\mathbf{k}. \tag{32}$$

4.2 Spatially concentrated bandlimited functions

We use $g(\mathbf{x})$ to denote a real function that is bandlimited to $\mathcal{K}$, an arbitrary subregion of spectral space,

$$g(\mathbf{x}) = (2\pi)^{-2}\int_{\mathcal{K}} G(\mathbf{k})e^{i\mathbf{k}\cdot\mathbf{x}}\,d\mathbf{k}, \tag{33}$$

Following Slepian (1964), we seek to concentrate the power of $g(\mathbf{x})$ into a finite spatial region $\mathcal{R} \subset \mathbb{R}^2$, of area A, by maximizing the energy ratio

$$\lambda = \frac{\int_{\mathcal{R}} g^2(\mathbf{x})\,d\mathbf{x}}{\int_{\mathbb{R}^2} g^2(\mathbf{x})\,d\mathbf{x}}. \tag{34}$$

Upon inserting the representation (33) of $g(\mathbf{x})$ into Eq. (34) we can express the concentration in the form of the Rayleigh quotient

$$\lambda = \frac{\int_{\mathcal{K}}\int_{\mathcal{K}} G^*(\mathbf{k})D(\mathbf{k},\mathbf{k}')G(\mathbf{k}')\,d\mathbf{k}\,d\mathbf{k}'}{\int_{\mathcal{K}} |G(\mathbf{k})|^2\,d\mathbf{k}}, \tag{35}$$

where we have used Parseval's relation (32) and defined the positive-definite quantity

$$D(\mathbf{k},\mathbf{k}') = (2\pi)^{-2}\int_{\mathcal{R}} e^{i(\mathbf{k}'-\mathbf{k})\cdot\mathbf{x}}\,d\mathbf{x}, \tag{36}$$

which is Hermitian, $D(\mathbf{k}, \mathbf{k}') = D^*(\mathbf{k}', \mathbf{k})$. Bandlimited functions $g(\mathbf{x})$ that maximize Eqs. (34)–(35) solve the Fourier-domain Fredholm integral equation

$$\int_{\mathcal{K}} D(\mathbf{k}, \mathbf{k}')G(\mathbf{k}')\, d\mathbf{k}' = \lambda G(\mathbf{k}), \quad \mathbf{k} \in \mathcal{K}. \tag{37}$$

Comparison of Eq. (36) with Eq. (31) leads to the interpretation of the spectral-domain kernel $D(\mathbf{k}, \mathbf{k}')$ as a spacelimited spectral delta function. We rank order the concentration eigenvalues so that $1 > \lambda_1 \geq \lambda_2 \geq \cdots > 0$. Upon multiplication of Eq. (37) with $e^{i\mathbf{k}\cdot\mathbf{x}}$ and integrating over all $\mathbf{k} \in \mathcal{K}$, we obtain the corresponding problem in the spatial domain as

$$\int_{\mathcal{R}} D(\mathbf{x}, \mathbf{x}')g(\mathbf{x}')\, d\mathbf{x}' = \lambda g(\mathbf{x}), \quad \mathbf{x} \in \mathbb{R}^2, \tag{38a}$$

$$D(\mathbf{x}, \mathbf{x}') = (2\pi)^{-2} \int_{\mathcal{K}} e^{i\mathbf{k}\cdot(\mathbf{x}-\mathbf{x}')}\, d\mathbf{k}. \tag{38b}$$

Comparison of Eq. (38b) with Eq. (29) shows that the Hermitian spatial-domain kernel $D(\mathbf{x}, \mathbf{x}') = D^*(\mathbf{x}', \mathbf{x})$ is a bandlimited spatial delta function. The bandlimited spatial-domain eigenfunctions $g_1(\mathbf{x}), g_2(\mathbf{x}), \ldots$ may be chosen to be orthonormal over the whole plane $\mathbb{R}^2$, in which case they are also orthogonal over the region $\mathcal{R}$:

$$\int_{\mathbb{R}^2} g_\alpha g_\beta\, d\mathbf{x} = \delta_{\alpha\beta}, \qquad \int_{\mathcal{R}} g_\alpha g_\beta\, d\mathbf{x} = \lambda_\alpha \delta_{\alpha\beta}. \tag{39}$$

In this normalization the eigenfunctions of Eq. (38) represent the kernel in (38b) as

$$D(\mathbf{x}, \mathbf{x}') = \sum_{\alpha=1}^{\infty} g_\alpha(\mathbf{x}) g_\alpha(\mathbf{x}'). \tag{40}$$

This form of Mercer's theorem (Flandrin 1998; Tricomi 1970) is verified by substituting the right hand side of Eq. (40) into Eq. (38a) and using the orthogonality (39).

4.3 Spectrally concentrated spacelimited functions

We use $h(\mathbf{x})$ to denote a function that is spacelimited, i.e. vanishes outside the arbitrary region $\mathcal{R}$ of physical space:

$$H(\mathbf{k}) = \int_{\mathcal{R}} h(\mathbf{x}) e^{-i\mathbf{k}\cdot\mathbf{x}}\, d\mathbf{x}. \tag{41}$$

To concentrate the energy of $h(\mathbf{x})$ into the finite spectral region $\mathcal{K}$, we maximize

$$\lambda = \frac{\int_{\mathcal{K}} |H(\mathbf{k})|^2 \, d\mathbf{k}}{\int_{\mathbb{R}^2} |H(\mathbf{k})|^2 \, d\mathbf{k}}. \tag{42}$$

Upon using Eq. (32) and inserting the representation (41) of $H(\mathbf{k})$ into Eq. (42) we can rewrite λ in the form

$$\lambda = \frac{\int_{\mathcal{R}} \int_{\mathcal{R}} h(\mathbf{x}) D(\mathbf{x}, \mathbf{x}') h(\mathbf{x}') \, d\mathbf{x} \, d\mathbf{x}'}{\int_{\mathcal{R}} h^2(\mathbf{x}) \, d\mathbf{x}}, \tag{43}$$

where we again encounter the quantity (38b),

$$D(\mathbf{x}, \mathbf{x}') = (2\pi)^{-2} \int_{\mathcal{K}} e^{i\mathbf{k}\cdot(\mathbf{x}-\mathbf{x}')} \, d\mathbf{k}. \tag{44}$$

Once again by Rayleigh's principle, spacelimited functions $h(\mathbf{x})$ that maximize the quotient λ in Eqs. (42)–(43) solve the spatial-domain Fredholm integral equation

$$\int_{\mathcal{R}} D(\mathbf{x}, \mathbf{x}') \, h(\mathbf{x}') \, d\mathbf{x}' = \lambda h(\mathbf{x}), \quad \mathbf{x} \in \mathcal{R}. \tag{45}$$

Equation (45) is identical to Eq. (38) save for the restriction to the domain $\mathcal{R}$. The eigenfunctions $h(\mathbf{x})$ that maximize the spectral norm ratio (42) are identical, within the region $\mathcal{R}$, to the eigenfunctions $g(\mathbf{x})$ that maximize the spatial norm ratio (34). The associated eigenvalues $1 > \lambda_1 \geq \lambda_2 \geq \cdots > 0$ are a measure both of the spatial concentration of $g(\mathbf{x})$ within the region $\mathcal{R}$ and of the spectral concentration of $h(\mathbf{x})$ to the wave vectors $\mathbf{k} \in \mathcal{K}$. Identifying

$$h(\mathbf{x}) = \begin{cases} g(\mathbf{x}) & \text{if } \mathbf{x} \in \mathcal{R}, \\ 0 & \text{otherwise}, \end{cases} \tag{46}$$

the normalization is such that

$$\int_{\mathbb{R}^2} h_\alpha h_\beta \, d\mathbf{x} = \int_{\mathcal{R}} h_\alpha h_\beta \, d\mathbf{x} = \lambda_\alpha \delta_{\alpha\beta}. \tag{47}$$

The null-space consisting of all non-bandlimited functions that have both no energy outside $\mathcal{R}$ nor inside $\mathcal{K}$ is of little consequence to us.

5 Slepian symmetry

Under what has been called "Slepian symmetry" (Brander and DeFacio 1986) the solutions to Eqs. (38) and (45) take on particularly attractive analytic forms. Anticipating a switch to polar coordinates $\mathbf{x} = (r, \theta)$ we introduce $J_m(k)$, the Bessel function of the first kind and of integer order m (Abramowitz and Stegun 1965; Gradshteyn and Ryzhik 2000). The Bessel functions satisfy the symmetry condition $J_{-m}(k) = (-1)^m J_m(k)$, the relation

$$1 = J_0^2(k) + 2\sum_{m=1}^{\infty} J_m^2(k) \tag{48}$$

and the identity (Jeffreys and Jeffreys 1988)

$$J_0(k\|\mathbf{x} - \mathbf{x}'\|) = J_0(kr)J_0(kr') + 2\sum_{m=1}^{\infty} J_m(kr)J_m(kr')\cos[m(\theta - \theta')]. \tag{49}$$

Furthermore, we have the particular formulas

$$J_0(k) = (2\pi)^{-1}\int_0^{2\pi} e^{ik\cos\theta}\, d\theta, \qquad J_1(k) = k^{-1}\int_0^{k} J_0(k')\, k'\, dk', \tag{50}$$

$$J_{1/2}(k) = \sqrt{\frac{2}{\pi k}}\,\sin k, \tag{51}$$

the derivative identity $\frac{d}{dk}[kJ_1(k)] = kJ_0(k)$ and the limits

$$\lim_{k\to 0}\frac{J_1(k)}{k} \to \frac{1}{2} \quad \text{and} \quad \lim_{k\to 0}\frac{J_m(k)}{\sqrt{k}} \to 0. \tag{52}$$

5.1 Circular bandlimitation

Limitation to the disk-shaped $\mathcal{K} = \{\mathbf{k} : \|\mathbf{k}\| \le K\}$ allows us to rewrite the spatial kernel of Eq. (44) using polar coordinates as follows. Letting $k = \|\mathbf{k}\| = (\mathbf{k}\cdot\mathbf{k})^{1/2}$ and θ be the angle between the wave vector $\mathbf{k}$ and the vector $\mathbf{x} - \mathbf{x}'$,

$$\mathbf{k}\cdot(\mathbf{x} - \mathbf{x}') = k\|\mathbf{x} - \mathbf{x}'\|\cos\theta, \tag{53}$$

and using Eq. (50), we obtain an expression alternative to Eq. (44) as

$$D(\mathbf{x},\mathbf{x}') = (2\pi)^{-2} \int_0^K \int_0^{2\pi} e^{ik\|\mathbf{x}-\mathbf{x}'\|\cos\theta}\, d\theta\, k\, dk, \tag{54a}$$

$$= (2\pi)^{-1} \int_0^K J_0(k\|\mathbf{x}-\mathbf{x}'\|)\, k\, dk, \tag{54b}$$

$$= \frac{K\, J_1(K\|\mathbf{x}-\mathbf{x}'\|)}{2\pi\, \|\mathbf{x}-\mathbf{x}'\|}. \tag{54c}$$

We notice the symmetry $D(\mathbf{x},\mathbf{x}') = D(\mathbf{x}',\mathbf{x}) = D(\|\mathbf{x}-\mathbf{x}'\|)$ and the equivalence of Eq. (54c) with the asymptotic expression (20b), as expected (Simons and Dahlen 2007; Simons et al. 2006). With Coifman and Lafon (2006) and through Eq. (51), we furthermore note that both Eqs. (54c) and (5b) are n-dimensional versions of the general form $[K/(2\pi)]^{n/2} J_{n/2}(K\|\mathbf{x}-\mathbf{x}'\|)/(\|\mathbf{x}-\mathbf{x}'\|^{n/2})$, for $n = 2$, and $n = 1$ (where $K = W$), respectively. As Eq. (52) now shows,

$$D(\mathbf{x},\mathbf{x}) = \frac{K^2}{4\pi}, \tag{55}$$

and thus Eqs. (39)–(40) allow us to write the sum of the concentration values λ as the "planar Shannon number"

$$N^{2\mathrm{D}} = \sum_{\alpha=1}^{\infty} \lambda_\alpha = \int_{\mathcal{R}} D(\mathbf{x},\mathbf{x})\, d\mathbf{x} = K^2\, \frac{A}{4\pi} = \frac{(\pi K^2)(A)}{(2\pi)^2}, \tag{56}$$

where A is the area of the spatial region of concentration $\mathcal{R}$. As in the one-dimensional case, Eq. (9), the Shannon number is equal to the area of the function in the spatiospectral phase plane times the "Nyquist density", as expected (Daubechies 1988, 1992). Roughly equal to the number of significant eigenvalues, $N^{2\mathrm{D}}$ again is the effective dimension of the space of "essentially" space- and bandlimited functions in which the reduced set of two-dimensional functions $g_1, g_2, \ldots, g_{N^{2\mathrm{D}}}$ may act as an efficient orthogonal basis. Using Eqs. (55) with (40) we furthermore see that the sum of the squares of all of the bandlimited eigenfunctions, independent of position $\mathbf{x}$ in the plane, is the constant

$$\sum_{\alpha=1}^{\infty} g_\alpha^2(\mathbf{x}) = \frac{K^2}{4\pi}. \tag{57}$$

Likewise, since the first $N^{2\mathrm{D}}$ eigenfunctions $g_1, g_2, \ldots, g_{N^{2\mathrm{D}}}$ have eigenvalues near unity and lie mostly within $\mathcal{R}$, and the remainder $g_{N^{2\mathrm{D}}+1}, g_{N^{2\mathrm{D}}+2}, \ldots, g_\infty$ have eigenvalues near zero and lie mostly outside $\mathcal{R}$ in $\mathbb{R}^2$, we expect the eigenvalue-weighted sum of squares to be

$$\sum_{\alpha=1}^{\infty}\lambda_\alpha g_\alpha^2(\mathbf{x}) \approx \sum_{\alpha=1}^{N^{2\mathrm{D}}}\lambda_\alpha g_\alpha^2(\mathbf{x}) \approx \begin{cases} N^{2\mathrm{D}}/A & \text{if } \mathbf{x}\in\mathcal{R}, \\ 0 & \text{otherwise.} \end{cases} \tag{58}$$

This heuristic finding is of great importance in the analysis and representation of signals using the Slepian functions as an approximate basis, as much as for their use as tapers to perform spectral analysis on data from which we thus expect to extract all relevant statistical information with minimal loss or leakage near the edges of the region under consideration (Walden 1990).

5.2 Scaling analysis I

Introducing scaled independent and dependent variables

$$\boldsymbol{\xi} = \sqrt{\frac{4\pi}{A}}\,\mathbf{x}, \quad \boldsymbol{\xi}' = \sqrt{\frac{4\pi}{A}}\,\mathbf{x}', \quad \psi(\boldsymbol{\xi}) = g(\mathbf{x}), \quad \psi(\boldsymbol{\xi}') = g(\mathbf{x}'), \tag{59}$$

we can rewrite Eqs. (38) and (54c) as

$$\int_{\mathcal{R}_*} D(\boldsymbol{\xi},\boldsymbol{\xi}')\,\psi(\boldsymbol{\xi}')\,d\boldsymbol{\xi}' = \lambda\,\psi(\boldsymbol{\xi}), \tag{60a}$$

with $\mathcal{R}_*$, of area 4π, the image of the concentration region $\mathcal{R}$ under (59), and

$$D(\boldsymbol{\xi},\boldsymbol{\xi}') = \frac{\sqrt{N^{2\mathrm{D}}}}{2\pi}\,\frac{J_1(\sqrt{N^{2\mathrm{D}}}\|\boldsymbol{\xi}-\boldsymbol{\xi}'\|)}{\|\boldsymbol{\xi}-\boldsymbol{\xi}'\|}. \tag{60b}$$

Equation (60) reveals that the eigenvalues $\lambda_1, \lambda_2, \ldots$ and the scaled eigenfunctions $\psi_1(\boldsymbol{\xi}), \psi_2(\boldsymbol{\xi}), \ldots$ depend on the maximum circular bandwidth K and the spatial concentration area A only through the planar Shannon number $N^{2\mathrm{D}}$, as they do in the one-dimensional, Eq. (8), and asymptotic spherical, Eq. (20), cases. Under this scaling the Shannon number remains

$$N^{2\mathrm{D}} = \int_{\mathcal{R}_*} D(\boldsymbol{\xi},\boldsymbol{\xi})\,d\boldsymbol{\xi} = \frac{N^{2\mathrm{D}}}{4\pi}\int_{\mathcal{R}_*} d\boldsymbol{\xi} = N^{2\mathrm{D}}. \tag{61}$$

5.3 Circular spacelimitation

If in addition to the circular spectral limitation, physical space is also circularly limited, in other words, if the spatial region of concentration or limitation $\mathcal{R}$ is a circle of

radius R, then a polar coordinate, $\mathbf{x} = (r, \theta)$, representation

$$g(r,\theta) = \begin{cases} \sqrt{2}\mathsf{g}(r)\cos(m\theta) & \text{if } m < 0, \\ \mathsf{g}(r) & \text{if } m = 0, \\ \sqrt{2}\mathsf{g}(r)\sin(m\theta) & \text{if } m > 0, \end{cases} \tag{62}$$

may be used to decompose Eq. (60) into an infinite series of non-degenerate fixed-order eigenvalue problems, one for each order $\pm m$. We do this most easily by inserting Eq. (49) into Eq. (54b), the obtained result with Eq. (62) into Eq. (38a), and using the orthogonality of the functions $\ldots, \sqrt{2}\cos(m\theta), \ldots, 1, \ldots, \sqrt{2}\sin(m\theta), \ldots$ over the polar angles $0 \le \theta < 2\pi$. The integral equation for the fixed-m radial function $\mathsf{g}(r)$ is then given by

$$\int_0^R D(r,r')\mathsf{g}(r')\,r'dr' = \lambda\,\mathsf{g}(r), \tag{63a}$$

with the fixed-m symmetric kernel

$$D(r,r') = K^2 \int_0^1 J_m(Kpr)\,J_m(Kpr')\,p\,dp. \tag{63b}$$

We rank order the distinct but pairwise occurring eigenvalues obtained by solving each of the fixed-order eigenvalue problems (63) so that $1 > \lambda_1 > \lambda_2 > \cdots > 0$, and we orthonormalize the associated eigenvectors $\mathsf{g}_1, \mathsf{g}_2, \ldots$ as in Eq. (39) so that

$$2\pi \int_0^\infty \mathsf{g}_\alpha(r)\mathsf{g}_\beta(r)\,r\,dr = \delta_{\alpha\beta}, \qquad 2\pi \int_0^R \mathsf{g}_\alpha(r)\mathsf{g}_\beta(r)\,r\,dr = \lambda_\alpha\delta_{\alpha\beta}. \tag{64}$$

We shall denote the radial part of the functions $h(r,\theta)$ by $\mathsf{h}(r)$ in Sect. 5.6.

5.4 Scaling analysis II

Finally, the scaling transformations

$$\xi = r/R, \quad \xi' = r'/R, \quad \psi(\xi) = \mathsf{g}(r), \quad \psi(\xi') = \mathsf{g}(r'), \tag{65}$$

convert Eq. (63) into the scaled eigenvalue problem

$$\int_0^1 D(\xi,\xi')\,\psi(\xi')\,\xi'd\xi' = \lambda\,\psi(\xi), \tag{66a}$$

with the fixed-m kernel

$$D(\xi,\xi') = 4N^{2D}\int_0^1 J_m(2\sqrt{N^{2D}}\,p\xi)\,J_m(2\sqrt{N^{2D}}\,p\xi')\,p\,dp, \tag{66b}$$

which is dependent only upon the Shannon number

$$N^{2D} = K^2\frac{R^2}{4}. \tag{67}$$

The number of significant eigenvalues per angular order m is (Simons and Dahlen 2007; Simons et al. 2006)

$$N_m^{2D} = \int_0^1 D(\xi,\xi)\xi\,d\xi = 4N^{2D}\int_0^1\int_0^1 J_m^2(2\sqrt{N^{2D}}\,p\xi)\,p\,dp\,\xi\,d\xi, \tag{68}$$

$$\begin{aligned}&= 2N^{2D}\left[J_m^2(2\sqrt{N^{2D}}) + J_{m+1}^2(2\sqrt{N^{2D}})\right]\\ &\quad -(2m+1)\sqrt{N^{2D}}J_m(2\sqrt{N^{2D}})J_{m+1}(2\sqrt{N^{2D}})\\ &\quad -\frac{m}{2}\left[1 - J_0^2(2\sqrt{N^{2D}}) - 2\sum_{n=1}^{m}J_n^2(2\sqrt{N^{2D}})\right].\end{aligned} \tag{69}$$

The complete Shannon number N^{2D} is preserved, inasmuch as, per Eqs. (68) and (48),

$$N^{2D} = N_0^{2D} + 2\sum_{m=1}^{\infty}N_m^{2D} = 4N^{2D}\int_0^1\int_0^1 p\,dp\,\xi\,d\xi = N^{2D}. \tag{70}$$

5.5 Sturm–Liouville character and tridiagonal matrix formulation

As noted by Slepian (1964), Eq. (66) is an iterated version of the equivalent "square-root" equation

$$2\sqrt{N^{2D}}\int_0^1 J_m(2\sqrt{N^{2D}}\,\xi\xi')\psi(\xi')\xi'd\xi' = \sqrt{\lambda}\,\psi(\xi). \tag{71}$$

To see this, it suffices to substitute for $\psi(\xi')$ on the left hand side of Eq. (71) using Eq. (71) itself. Thus, the eigenvalues $\lambda_1, \lambda_2, \ldots$ and eigenfunctions $\psi_1(\xi), \psi_2(\xi), \ldots$ of Eq. (66) may alternatively be found by solving the equivalent equation (71). A further reduction can be obtained by substituting a scaled Shannon number or bandwidth and rescaling,

$$c = 2\sqrt{N^{2\mathrm{D}}}, \quad \gamma = \sqrt{\lambda}/\sqrt{c}, \quad \varphi(\xi) = \sqrt{\xi}\,\psi(\xi), \tag{72}$$

to yield the more symmetric form

$$\int_0^1 J_m(c\xi\xi')\sqrt{c\xi\xi'}\,\varphi(\xi')\,d\xi' = \gamma\,\varphi(\xi). \tag{73}$$

On the domain $0 \le \xi \le 1$ the $\varphi(\xi)$ also solve a Sturm–Liouville equation,

$$\frac{d}{d\xi}\left[(1-\xi^2)\frac{d\varphi}{d\xi}\right] + \left(\chi + \frac{1/4 - m^2}{\xi^2} - 4N^{2\mathrm{D}}\xi^2\right)\varphi = 0, \quad |\xi| \le 1, \tag{74}$$

for some $\chi \neq \lambda$. When $m = \pm 1/2$ Eq. (74) reduces to the one-dimensional equation (11), as can be seen by comparing Eqs. (67) and (9) after making the identifications $K = W$ and $R = T$. The fixed-m Slepian functions $\varphi(\xi)$ can be determined by writing them as the infinite series

$$\varphi(\xi) = m!\,\xi^{m+\frac{1}{2}} \sum_{l=0}^{\infty} \frac{d_l\, l!}{(l+m)!} P_l^{m0}(1-2\xi^2), \quad 0 \le \xi \le 1, \tag{75}$$

whereby the $P_l^{m0}(x)$ are the Jacobi polynomials (Abramowitz and Stegun 1965):

$$P_l^{m0}(x) = \frac{(l+m)!\,l!}{2^l} \sum_{n=0}^{l} \frac{(x-1)^n (x+1)^{l-n}}{(n+m)!(l-n)!^2 n!}. \tag{76}$$

By extension to $\xi > 1$ they can also be determined from the rapidly converging Bessel series

$$\varphi(\xi) = \frac{m!}{\gamma} \sum_{l=0}^{\infty} \frac{d_l\, l!}{(l+m)!} \frac{J_{m+2l+1}(c\xi)}{\sqrt{c\xi}}, \quad \xi \in \mathbb{R}^+. \tag{77}$$

From Eq. (52) we confirm that $\varphi(0) = 0$. In both cases, the required fixed-m expansion coefficients d_l can be determined by recursion (Bouwkamp 1947; Slepian 1964), which is, however, rarely stable. It is instead more practical to determine them as the eigenvectors of the non-symmetric tridiagonal matrix (de Villiers et al. 2003; Shkolnisky 2007) that is the spectral form, with the same eigenvalues, of Eq. (74),

$$T_{l+1\,l} = -\frac{c^2\,(m+l+1)^2}{(2l+m+1)(2l+m+2)}, \tag{78a}$$

$$T_{ll} = \left(2l+m+\frac{1}{2}\right)\left(2l+m+\frac{3}{2}\right) + \frac{c^2}{2}\left[1+\frac{m^2}{(2l+m)(2l+m+2)}\right], \tag{78b}$$

$$T_{l\,l+1} = -\frac{c^2(l+1)^2}{(2l+m+2)(2l+m+3)}, \tag{78c}$$

where the parameter l ranges from 0 to some large value that ensures convergence. Finally, the desired concentration eigenvalues λ can subsequently be obtained by direct integration of Eq. (60), or, alternatively (Slepian 1964), from

$$\lambda = 2\gamma^2\sqrt{N^{2\mathrm{D}}}, \quad \text{with} \quad \gamma = \frac{c^{m+1/2}d_0}{2^{m+1}(m+1)!}\left(\sum_{l=0}^{\infty} d_l\right)^{-1}. \tag{79}$$

Neither procedure is particularly accurate for small values λ, though these will be rarely needed in applications. A more uniformly valid stable recursive scheme is described elsewhere (Slepian and Pollak 1961; Xiao et al. 2001). The overall accuracy of the procedures chosen can be verified with the aid of the exact formula Eq. (69), as for the fixed-m eigenvalues, $N_m^{2\mathrm{D}} = \sum_{\alpha=1}^{\infty}\lambda_\alpha$.

5.6 Numerical examples

With the eigenfunctions $\varphi(\xi)$ calculated, by series expansion (de Villiers et al. 2003; Shkolnisky 2007) via Eqs. (75) or (77) or even by quadrature (Zhang 1994) of Eq. (73), we rescale them following Eqs. (72) and (65) to the Slepian functions $\mathsf{g}_\alpha(r)$ normalized according to (64). The sign is arbitrary: the concentration criterion is a quadratic.

The four most optimally concentrated eigenfunctions $\mathsf{g}_1(r)$, $\mathsf{g}_2(r)$, $\mathsf{g}_3(r)$, $\mathsf{g}_4(r)$, for the orders $0 \le m \le 4$ are plotted in Fig. 1, scaled for convenience. The associated eigenvalues $\lambda_1, \lambda_2, \lambda_3, \lambda_4$ are listed to six-figure accuracy. The planar Shannon number in this example is $N^{2\mathrm{D}} = 42$, hence $c \approx 13$. It is useful to compare the behavior of these solutions to those of the spherical concentration problem (Simons et al. 2006, Fig. 5.1), with which they are asymptotically self-similar (Simons and Dahlen 2007; Simons et al. 2006). The first zeroth-order "zonal" ($m = 0$) eigenfunction, $\mathsf{g}_1(r)$, has no nodes within the "cap" of radius R; the second, $\mathsf{g}_2(r)$, has one node, and so on. The non-zonal ($m > 0$) eigenfunctions all vanish at the origin. The first three $m = 0$, $m = 1$ and $m = 2$, and the first two $m = 3$ and $m = 4$ eigenfunctions are very well concentrated ($\lambda > 0.9$). The fourth $m = 3$ and $m = 4$ eigenfunctions exhibit significant leakage ($\lambda < 0.1$).

The squared Fourier coefficients $|H(k)|^2$ of the four best concentrated spacelimited eigenfunctions $\mathsf{h}_1(r)$, $\mathsf{h}_2(r)$, $\mathsf{h}_3(r)$, $\mathsf{h}_4(r)$ for $0 \le m \le 4$ are plotted versus scaled wavenumber $\kappa = k/c$, on a decibel scale, in Fig. 2. Shannon number, bandwidth, and layout are the same as in Fig. 1. See elsewhere (Simons et al. 2006, Fig. 5.2) to compare with the spherical case.

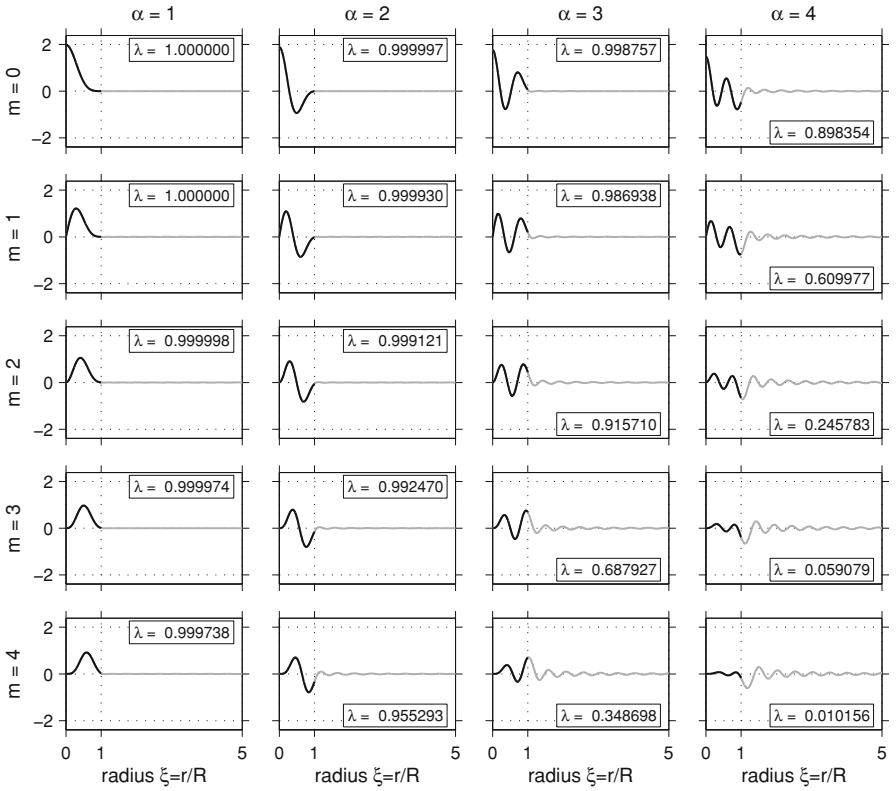

Fig. 1 Radial dependence of the first four eigenfunctions of Eq. (63), the bandlimited Slepian functions $\mathsf{g}_\alpha(r)$, $\alpha = 1, 2, 3, 4$, of fixed order $m = 0$ (*top*) to $m = 4$ (*bottom*), calculated from Eq. (77) truncated at $l = 84$. The Shannon number $N^{2\mathrm{D}} = 42$ and the bandwidth $c \approx 13$. *Black curves* show the concentration within the scaled spatial interval $0 \leq \xi \leq 1$ and *grey curves* show the leakage into the rest of the real line, which is truncated at $\xi = 5$. *Labels* show the eigenvalues, λ_α, calculated from Eq. (79). These express the quality of the spatial concentration. Spacelimited, spectral-domain Slepian functions are shown in Fig. 2

Once a number of sequences of fixed-order eigenvalues has been found, they can be resorted to an overall mixed-order ranking. The total number of significant eigenvalues is then given by Eq. (70). In Fig. 3 we show the mixed-m eigenvalue spectra for the Shannon numbers $N^{2\mathrm{D}} = 3$, 11, 24 and 42. These show the familiar step shape (Landau 1965; Slepian and Sonnenblick 1965), with significant ($\lambda \approx 1$) and insignificant ($\lambda \approx 0$) eigenvalues separated by a narrow transition band. The Shannon numbers roughly separate the reasonably well concentrated eigensolutions ($\lambda \geq 0.5$) from the more poorly concentrated ones ($\lambda < 0.5$) in all four cases. To compare with the spherical case, see elsewhere (Simons et al. 2006, Fig. 5.3).

Finally, Fig. 4 shows a polar plot of the first 30 eigenfunctions $g(r, \phi)$ concentrated within a radius $R = 1$, defined by Eqs. (62) using the $\mathsf{g}(r)$ shown in Fig. 1. The Shannon number is $N^{2D} = 42$, as in Fig. 1. The eigenvalue ranking is mixed-order, as in Fig. 3, and all degenerate $\sqrt{2}\cos(m\phi)$, $\sqrt{2}\sin(m\phi)$ doublets are shown. The concentration factors $1 > \lambda \geq 0.8983$ and orders m of each eigenfunction are indicated. Blue

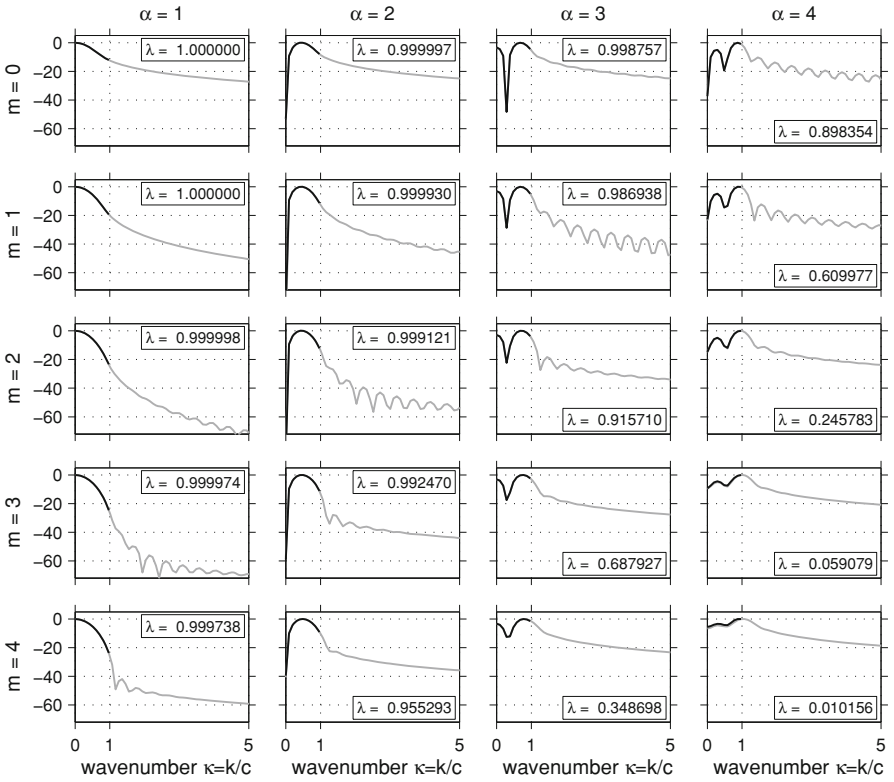

Fig. 2 Squared Fourier coefficients $|H(k)|^2$ of the first four scaled spacelimited eigenfunctions $\mathsf{h}_\alpha(r)$, $\alpha = 1, 2, 3, 4$, of fixed order $m = 0$ (*top*) to $m = 4$ (*bottom*), calculated by discrete Fourier transformation of the functions shown by the *thick black lines* in Fig. 1. The Shannon number is $N^{2\mathrm{D}} = 42$ and the scaled bandwidth $c \approx 13$. *Black curves* show the power within the scaled wavenumber interval $0 \le \kappa \le 1$ and *grey curves* show the power leaked to the rest of the wavenumber axis, which is truncated at $\kappa = 5$. Values of $|H(k)|^2$ are in decibel (dB), zero at the individual maxima. *Labels* show the eigenvalues λ_α, which express the quality of the spectral concentration. The corresponding bandlimited, spatial-domain eigenfunctions are shown in Fig. 1

and red colors (in the online version; in print these have been converted to grey scales between white and black) represent positive and negative values, respectively; however, all signs could be reversed without violating the quadratic concentration criteria (34) and (42). Elsewhere (Simons et al. 2006, Fig. 5.4) these can be compared with the spherical case. Other calculation methods (see Sect. 6 below) may yield slight differences between what should be pairs of eigenvalues for each non-azimuthally symmetric and thus fixed non-zero order eigenfunction. The mismatch is confined to the last two quoted digits in a typical calculation (compare Simons 2010, Fig. 2).

6 Computational considerations on general domains

While the framework of Sect. 4 is completely nonrestrictive as to the geometry of the spectral or spatial concentration regions $\mathcal{K}$ or $\mathcal{R}$, the literature treatment has remained

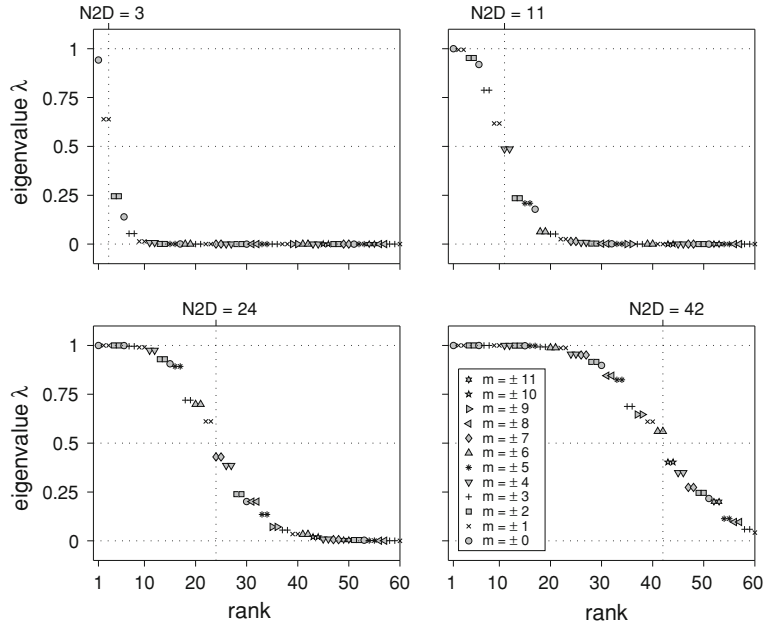

Fig. 3 Eigenvalue spectra (λ_α vs. rank α) of the Cartesian concentration problem, at various Shannon numbers N^{2D}, for disk-shaped regions, calculated via Eq. (79). The total number of eigenvalues is unbounded; only λ_1 through λ_{60} are shown. *Different symbols* are used to plot the various orders $-11 \leq m \leq 11$; *juxtaposed identical symbols* are $\pm m$ doublets. *Vertical grid lines* and *top labels* specify the rounded Shannon numbers $N^{2D} = 3, 11, 24, 42$

focused on the cases with special symmetry that we discussed in Sect. 5, for which analytic solutions could be found. In what follows we lift all such restrictions and, numerically, solve the problem of finding the unknown planar function $f(\mathbf{x})$ that is bandlimited/band-concentrated to $\mathcal{K}$ and space-concentrated/spacelimited to $\mathcal{R}$, by satisfying the Fredholm eigenvalue equation

$$\int_{\mathcal{R}} D(\mathbf{x}, \mathbf{x}') f(\mathbf{x}')\, d\mathbf{x}' = \lambda f(\mathbf{x}), \tag{80a}$$

$$D(\mathbf{x}, \mathbf{x}') = (2\pi)^{-2} \int_{\mathcal{K}} e^{i\mathbf{k}\cdot(\mathbf{x}-\mathbf{x}')}\, d\mathbf{k}, \tag{80b}$$

over the domains $\mathbf{x} \in \mathbb{R}^2$ (in which case we retrieve the bandlimited Slepian functions g of Sect. 4.2) or $\mathbf{x} \in \mathcal{R}$ (when we obtain the spacelimited h of Sect. 4.3).

6.1 Isotropic spectral response

Despite the appealing generality of Eq. (80), applications in the geophysical or planetary sciences, e.g. in problems of spectral analysis of data collected on bounded

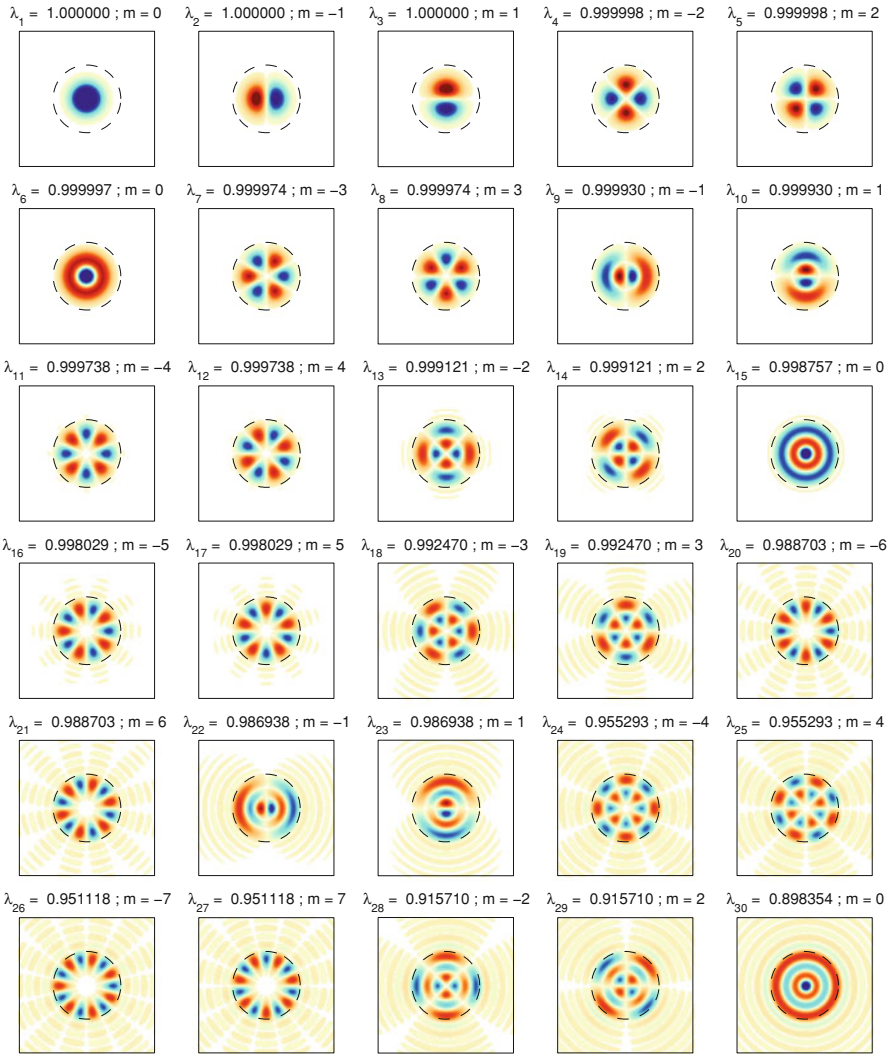

Fig. 4 Bandlimited eigenfunctions $g(r, \theta)$ that are optimally concentrated within a disk of radius $R = 1$. *Dashed circle* denotes the region boundary. The Shannon number $N^{\mathrm{2D}} = 42$ and the scaled bandwidth $c \approx 13$. The eigenvalues λ_α have been sorted into a mixed-order ranking, $\alpha = 1 \rightarrow 30$, with the best concentrated eigenfunction plotted on the *top left* and the 30th best on the *lower right*. Blue (or *white* in the print version) is positive and red (*black* in print) is negative; regions in which the absolute value is less than one hundredth of the maximum value on the domain are left white (*grey* at 50% in the print version)

geographical domains, is well served by Slepian functions whose spectral support is circularly isotropic. As we saw in Sect. 5.1, the integral kernel is then

$$D(\mathbf{x}, \mathbf{x}') = \frac{K\, J_1(K\,\|\mathbf{x} - \mathbf{x}'\|)}{2\pi\,\|\mathbf{x} - \mathbf{x}'\|}. \tag{81}$$

The standard solution to solve homogeneous Fredholm integral equations of the second kind is by the Nyström method (Nyström 1930; Press et al. 1992).

In one dimension, let us write Eq. (80) in a form reminiscent of the special case that we encountered previously in Eq. (63), to which it also applies explicitly, namely

$$\int_a^b D(x, x')\, f(x')\, dx' = \lambda f(x). \tag{82}$$

The left-hand side of this equation is to be discretized by a quadrature rule; this involves choosing J weights w_j and abscissas x_j such that, to the desired accuracy,

$$\int_a^b D(x, x')\, f(x')\, dx' = \sum_{j=1}^{J} w_j D(x, x_j)\, f(x_j), \tag{83}$$

using which we rewrite Eq. (82) as

$$\sum_{j=1}^{J} w_j D(x_i, x_j)\, f(x_j) = \lambda f(x_i), \tag{84}$$

this time evaluating the unknown right hand side $f(x)$ at the quadrature points as well. Written in matrix form, we may solve

$$\mathbf{D} \cdot \mathbf{W} \cdot \mathbf{f} = \lambda \mathbf{f}, \tag{85}$$

identifying the elements of the square kernel $D_{ij} = D(x_i, x_j)$, the samples of the unknown function as $f_j = f(x_j)$, and the entries of the diagonal weight matrix $W_{ij} = w_j \delta_{ij}$.

Restoring the symmetry of the problem contained in the symmetry $\mathbf{D} = \mathbf{D}^{\mathrm{T}}$, and provided the weights w_j are positive, we had rather solve

$$\tilde{\mathbf{W}} \cdot \mathbf{D} \cdot \tilde{\mathbf{W}} \cdot \tilde{\mathbf{f}} = \lambda \tilde{\mathbf{f}}, \tag{86}$$

using $\tilde{W}_{ij} = \sqrt{w_i}\delta_{ij}$ and $\tilde{\mathbf{f}} = \tilde{\mathbf{W}} \cdot \mathbf{f}$ or indeed $\tilde{f}_i = \sqrt{w_i} f_i$. Having solved this system for the unknown function $f(x_i)$ at the integration nodes, we can subsequently produce either $g(x)$ (anywhere in one-dimensional space) or $h(x)$ (inside the region) using Eqs. (82)–(83), to the same accuracy.

In two dimensions, the vectors $\mathbf{x} = (x, y)$ and $\mathbf{x}' = (x', y')$ denote points occupying the plane and Eq. (80) is rewritten as

$$\int_{\mathcal{R}} D(\mathbf{x}, \mathbf{x}')\, f(\mathbf{x}')\, d\mathbf{x}' = \sum_{k=1}^{K} \sum_{l=1}^{L} w_k w_l D(\mathbf{x}; x_k, y_l) f(x_k, y_l), \tag{87}$$

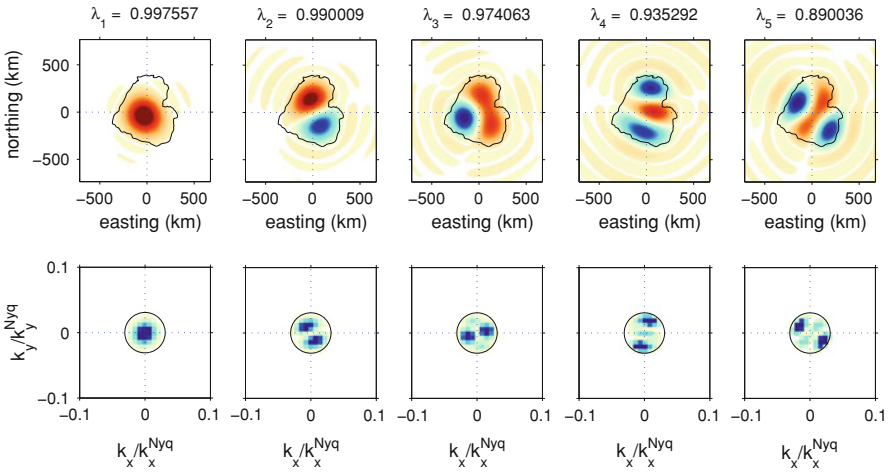

Fig. 5 Bandlimited eigenfunctions $g_1, g_2, \ldots, g_5$, calculated by Eq. (88) using Gauss–Legendre integration with 32 node points in both directions, optimally concentrated within the Colorado Plateaus, centered on 109.95°W 37.01°N (near Mexican Hat, UT) of area $A \approx 334 \times 10^3$ km^2. The concentration factors $\lambda_1, \lambda_2, \ldots, \lambda_5$ are indicated; the Shannon number is $N^{2D} = 10$. The *top row* renders the eigenfunctions in space on a grid with 5 km resolution in both directions, with the reversible convention that positive values are blue (*white* in print) and negative values red (*black* in print). The spatial concentration region is outlined in *black*. The *bottom row* shows the squared Fourier coefficients $|G(\mathbf{k})|^2$ as calculated from the functions $g(\mathbf{x})$ shown, on a wavenumber scale that is expressed as a fraction of the Nyquist wavenumber. The spectral limitation region is shown by the *black circle* at wavenumber $K = 0.0194$ rad/km. All areas for which the absolute value of the functions plotted is less than one hundredth of the maximum value attained over the domain are left white (*grey* at 50% in the print version)

where it is implied that $w_l = w_l(x_k)$ and $y_l = y_l(x_k)$. By wrapping the indices k and l on the scalar elements x' and y' into the vectorial indices i and j used for $\mathbf{x}$ and $\mathbf{x}'$ we arrive at

$$\sum_{j=1}^{J} w'_j D(\mathbf{x}_i; \mathbf{x}_j) f(\mathbf{x}_j) = \lambda f(\mathbf{x}_i). \tag{88}$$

This is identical to Eq. (86) as long as we remember that the weights w'_j are pairwise products of the one-dimensional $w_k w_l$ and identifying $D_{ij} = D(\mathbf{x}_i; \mathbf{x}_j)$.

As to the choice of quadrature, a finely meshed Riemann sum might suffice for some applications (Saito 2007; Zhang 1994), though we shall prefer the classical Gauss–Legendre algorithm (Press et al. 1992) for increased accuracy at faster computation speeds. Other options are available as well (Ramesh and Lean 1991). The analytical formulas for the special cases, e.g. Eqs. (75), (77) and (79) can be used for verification purposes (see the discussion of Fig. 4 in the text), as we have.

Figures 5 and 6 were computed using Eq. (88) with Gauss–Legendre quadrature, starting from a splined boundary of the Colorado Plateaus, a physiographic region in the United States. Figure 5 shows the first five bandlimited Slepian functions, $g_1 \to g_5$, with their eigenvalues, $\lambda_1 \to \lambda_5$. The space-domain functions $g(\mathbf{x})$, shown in the top row, are increasingly oscillatory as their concentration values decrease. At the same

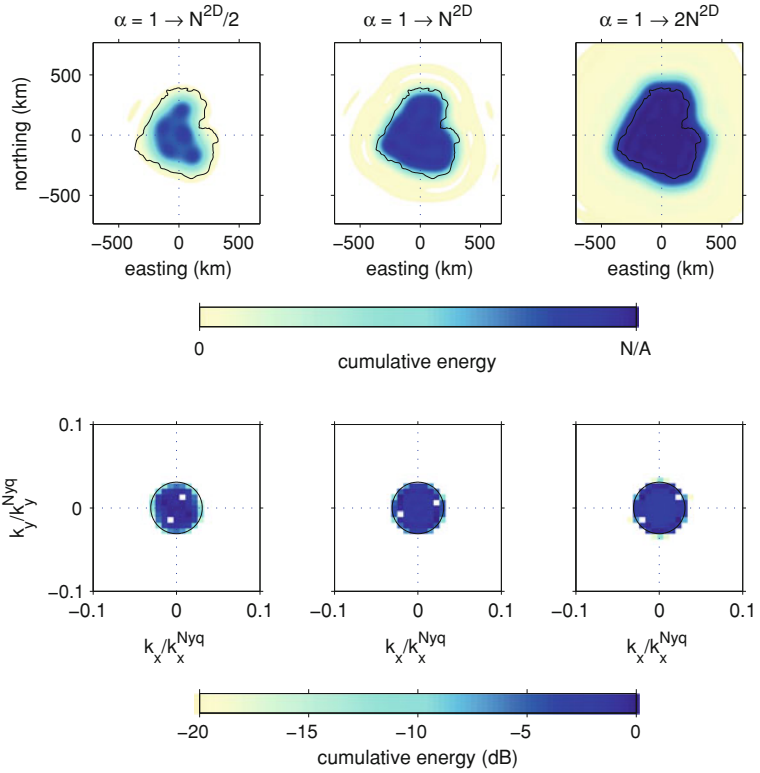

Fig. 6 Cumulative eigenvalue-weighted energy of the first $N^{2D}/2$, N^{2D} and $2N^{2D}$ eigenfunctions that are optimally concentrated within the Colorado Plateaus, with the Shannon number $N^{2D} = 10$. The *top row* is in the spatial domain with the concentration region outlined in *black*. Darkest blue (*white* in print) on color bar corresponds to the expected value (58) of the sum, as shown. The *bottom row* is in the spectral domain with a wavenumber scale that is expressed as a fraction of the Nyquist wavenumber. The spectral limitation region is shown by the *black circle*. Areas with absolute value less than one hundredth of the maximum value attained over the domain are left white (*grey* at 50% in the print version)

time their periodograms $|G(\mathbf{k})|^2$, shown in the bottom row, remain strictly confined within the chosen isotropic spectral region of bandwidth K. All together, the Slepian functions uniformly occupy their respective domains of concentration or limitation. Figure 6 shows the eigenvalue-weighted partial sums of the energy of the eigenfunctions, in space (top row) and spectral space (bottom row). The progressive covering behavior, consistent with Eq. (58), lies at the basis of the success of the Slepian functions in being used as data tapers for spectral analysis (Bronez 1988; Liu and van Veen 1992; Percival and Walden 1993): orthogonal over the domain that they cover, smoothly but rapidly decaying to zero at the boundary of interest, and with a finite and isotropic spectral response.

6.2 Arbitrary spectral response

We finally treat the situation in which both the spatial and spectral concentration domains are of arbitrary description—but with Hermitian spectral symmetry, see

Eqs. (28)–(29), if the Slepian functions are to be real-valued. No analytical results can be expected for such a case, and we benefit from writing the concentration problem in its most abstract form. Writing $\mathcal{Q}$ for the operator that acts on a spatial function $f(\mathbf{x})$ to return its Fourier transform $F(\mathbf{k})$, we introduce the spatial projection operator

$$\mathcal{P}f(\mathbf{x}) = \begin{cases} f(\mathbf{x}) & \text{if } \mathbf{x} \in \mathcal{R}, \\ 0 & \text{otherwise}, \end{cases} \tag{89}$$

and the spectral projection operator

$$\mathcal{L}F(\mathbf{k}) = \begin{cases} F(\mathbf{k}) & \text{if } \mathbf{k} \in \mathcal{K}, \\ 0 & \text{otherwise}. \end{cases} \tag{90}$$

We rewrite the variational equations (34) and (42) in inner-product notation as

$$\lambda = \frac{\langle \mathcal{P}\mathcal{Q}^{-1}\mathcal{L}F, \mathcal{P}\mathcal{Q}^{-1}\mathcal{L}F \rangle}{\langle \mathcal{Q}^{-1}\mathcal{L}F, \mathcal{Q}^{-1}\mathcal{L}F \rangle} = \frac{\langle \mathcal{L}\mathcal{Q}\mathcal{P}f, \mathcal{L}\mathcal{Q}\mathcal{P}f \rangle}{\langle \mathcal{Q}\mathcal{P}f, \mathcal{Q}\mathcal{P}f \rangle} = \text{maximum}. \tag{91}$$

The associated spectral-domain and spatial-domain eigenvalue equations are

$$\mathcal{L}\mathcal{Q}\mathcal{P}\mathcal{Q}^{-1}\mathcal{L}(\mathcal{L}F) = \lambda(\mathcal{L}F), \qquad \mathcal{P}\mathcal{Q}^{-1}\mathcal{L}\mathcal{Q}\mathcal{P}(\mathcal{P}f) = \lambda(\mathcal{P}f), \tag{92}$$

where we have made use of the fact that $\mathcal{P}^2 = \mathcal{P}$ and $\mathcal{L}^2 = \mathcal{L}$ are self-adjoint, and that $\mathcal{Q}$ and $\mathcal{Q}^{-1}$ are each other's adjoints, provided we rewrite Eq. (28) as a unitary transform. In our notation, the solutions $\mathcal{L}F$ yield the Fourier transforms of the band-limited functions $g(\mathbf{x})$ of Sect. 4.2, while the $\mathcal{P}f$ represent the spacelimited functions $h(\mathbf{x})$ of Sect. 4.3.

For computation in the discrete-discrete case, $\mathcal{P}$ and $\mathcal{L}$ will simply be matrices of ones and zeros, and $\mathcal{Q}$ and $\mathcal{Q}^{-1}$ will be the discrete Fourier transform (DFT) matrix and its conjugate transpose. Both $\mathcal{L}\mathcal{Q}\mathcal{P}\mathcal{Q}^{-1}\mathcal{L}$ and $\mathcal{P}\mathcal{Q}^{-1}\mathcal{L}\mathcal{Q}\mathcal{P}$ will be Hermitian and typically sparse, hence a number of dedicated eigenvalues solvers can be used to find the Slepian functions. In our own MATLAB implementation we furthermore take advantage of defining the operators as "anonymous" functions. This greatly improves the performance of the resulting algorithm, which we tested by comparison with the methods available for the special cases discussed in Sects. 2 and 5. With this we have complete liberty to design Slepian functions on geographical domains, including the ability to construct "steerable", anisotropic windows for texture-sensitive analysis that is of interest in theory (Olhede and Metikas 2009; Van De Ville and Unser 2008) and practice (Audet and Mareschal 2007; Kirby and Swain 2006). Figure 7 shows two numerical examples of Slepian functions h spectrally sensitive in wedge-shaped oriented domains. The top row shows $h_1 \rightarrow h_4$ and their eigenvalues, $\lambda_1 \rightarrow \lambda_4$, followed by eigenvalue-weighted sums of their periodograms, $\sum_{\alpha=1}^{20} \lambda_\alpha |H_\alpha(\mathbf{k})|^2$, on a decibel scale. These are orientated at $\pi/6$ from the horizontal. The bottom row shows the equivalent results oriented at $-\pi/6$ from the horizontal. Both cases were computed by diagonalization (`eigs`) of the operator $\mathcal{P}\mathcal{Q}^{-1}\mathcal{L}\mathcal{Q}\mathcal{P}$ whereby $\mathcal{Q}$ is the anonymous function call to the two-dimensional Fast Fourier Transform (`fft2`) and

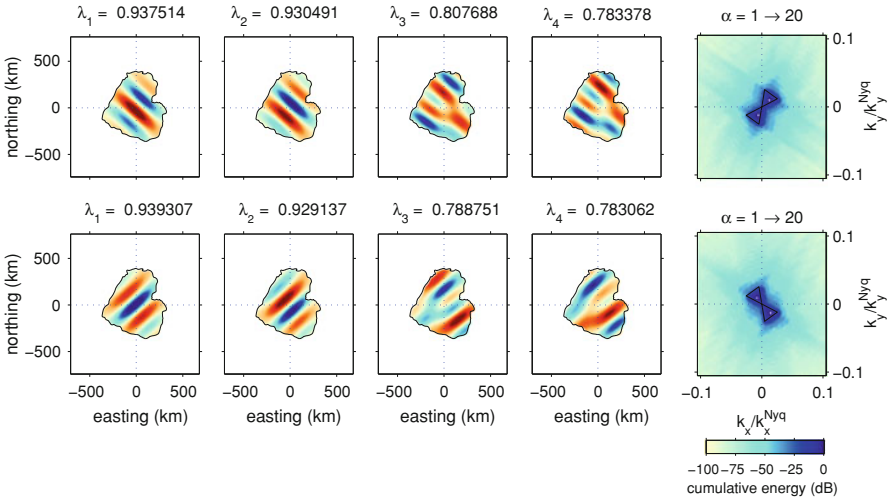

Fig. 7 Two sets of eigenfunctions $h_1, h_2, \ldots, h_4$ that are strictly spacelimited within the Colorado Plateaus and optimally concentrated within a wedge-shaped spectral domain, with their concentration factors $\lambda_1, \lambda_2, \ldots, \lambda_4$. The *last panel on each row* shows the eigenvalue-weighted periodograms of the first $\alpha = 1 \rightarrow 20$ eigenfunctions. The functions $h(\mathbf{x}) = \mathcal{P} f(\mathbf{x})$ were calculated by diagonalization of the spatial-domain operator equation (92) on a domain that we took to be three times the size of the box inscribing the concentration domain outlined in black, discretized on a 5×5 km^2 grid. The spectral concentration domains are *triangles* with Hermitian symmetry oriented at $\pm\pi/6$ from the *horizontal* in the *top and bottom rows*, respectively

$\mathcal{Q}^{-1}$ its inverse (`ifft2`). This immediately returns the $h(\mathbf{x})$ on a discretized calculation domain in which, once again, the region of the Colorado Plateaus was embedded. The functions $h_1 \rightarrow h_4$ shown are the real parts of the eigensolutions associated with the four eigenvalues $\lambda_1 \rightarrow \lambda_4$ that have the largest real part. The eigenvalues of these "generalized prolate spheroidal data sequences" (gpss), which need not in principle be defined on regularly sampled grids (Bronez 1988), are sensitive to the discretization and the size of the computational domains to which the inner products in Eq. (91) refer. The slightly different manner in which these sample the parametrically defined rotated spectral concentration domains explains the discrepancy of the eigenvalues between the two cases that are shown in the top and bottom rows of Fig. 7.

7 Conclusion

Slepian functions are orthogonal families of functions that are all defined on a common spatial domain, where they are either optimally concentrated or within which they are exactly limited. At the same time they are exactly confined within a certain spectral interval, or maximally concentrated therein (Simons 2010). The joint optimization of quadratic spatio-spectral concentration is generally referred to as Slepian's problem, which we encountered as Eq. (3) in one dimension, as Eq. (15) on the surface of a sphere, and as Eq. (34) in two Cartesian dimensions. Without qualification in one, and under special symmetry considerations in multiple dimensions, Slepian functions

solve Sturm–Liouville equations, notably Eqs. (11), (24), (26) and (74). In those cases (though on the sphere only asymptotically) the solutions depend on the spatial and spectral areas of concentration only through the Shannon number, which depends on their product, as defined by Eqs. (9), (21) and (56). More generally, they solve Fredholm integral equations in their respective dimensions, as exemplified by Eqs. (5), (17), and (38).

What unites the Slepian functions is that the kernels of the integral equations they solve are best thought of in the context of reproducing-kernel Hilbert spaces (Amirbekyan et al. 2008; Nashed and Walter 1991; Yao 1967). Each of $D(t,t')$ in Eq. (5b), $D(\hat{\mathbf{r}},\hat{\mathbf{r}}')$ in Eq. (17b) and $D(\mathbf{x},\mathbf{x}')$ in Eq. (38b), is a restriction of the traditional Dirac delta functions, $\delta(t,t')$, $\delta(\hat{\mathbf{r}},\hat{\mathbf{r}}')$, and $\delta(\mathbf{x},\mathbf{x}')$, to a region of finite bandwidth (Simons 2010). While the latter satisfy, for any square-integrable function f, the relations

$$f(t) = \int_{-\infty}^{\infty} f(t')\,\delta(t,t')\,dt', \tag{93a}$$

$$f(\mathbf{x}) = \int_{\mathbb{R}^2} f(\mathbf{x}')\,\delta(\mathbf{x},\mathbf{x}')\,d\mathbf{x}', \tag{93b}$$

$$f(\hat{\mathbf{r}}) = \int_{\Omega} f(\hat{\mathbf{r}}')\,\delta(\hat{\mathbf{r}},\hat{\mathbf{r}}')\,d\Omega', \tag{93c}$$

the former act on functions g that belong to appropriately bandlimited subspaces, as we have defined them in Eqs. (2), (14) and (33), in much the same way:

$$g(t) = \int_{-\infty}^{\infty} g(t')D(t,t')\,dt', \tag{94a}$$

$$g(\mathbf{x}) = \int_{\mathbb{R}^2} g(\mathbf{x}')D(\mathbf{x},\mathbf{x}')\,d\mathbf{x}', \tag{94b}$$

$$g(\hat{\mathbf{r}}) = \int_{\Omega} g(\hat{\mathbf{r}}')D(\hat{\mathbf{r}},\hat{\mathbf{r}}')\,d\Omega. \tag{94c}$$

Note that these are *not* equal to Eqs. (5), (17), or (38). Hence the g are a basis for bandlimited processes anywhere on the applicable domain ($\mathbb{R}$, $\mathbb{R}^2$ or the entire spherical surface Ω) (Daubechies 1992; Flandrin 1998; Freeden et al. 1998; Landau and Pollak 1961; Slepian and Pollak 1961). Therein, the Shannon-number best time- or space-concentrated members allow for sparse, approximate expansions of signals that are concentrated to the spatial region of choice. Similarly, the infinite sets of exactly time- or spacelimited (and thus band-concentrated) functions h which are the eigenfunctions of Eqs. (5), (17) and (38) with the domains appropriately restricted, see Eq. (45) for the two-dimensional case, are complete bases for square-integrable scalar functions on the intervals to which they are confined (Landau and Pollak 1961; Simons et al.

2006; Slepian and Pollak 1961). Expansions of wideband but spectrally concentrated signals in the small subset of their Shannon-number most band-concentrated members provide approximations which are spectrally faithful and constructive as their numbers grow (Simons 2010; Simons et al. 2009).

Slepian functions defined on two-dimensional Cartesian domains are of great utility in the natural sciences. Despite this, no comprehensive prior treatment was available, beyond that of cases for regions with advanced symmetry. The present paper has attempted to do right by, especially, the geosciences, where Fourier-based methods and analyses are often required but the domains of interest are rarely circles or rectangles. Much can be learned from those special cases, however, including from the one-dimensional and spherical situations that we have reviewed also. Most particularly, they have helped us test and benchmark the algorithms that we have discussed and are making available on the Web as part of this publication. In having ended Sect. 6 with a computational procedure for the design of planar Cartesian Slepian functions on arbitrarily irregular spatial and spectral domains, which could be captured in just a few lines, see Eqs. (89)–(92), and carried out in a handful of lines of MATLAB code, we believe to have returned to a level of practicality that should appeal to researchers across a wide spectrum.

Acknowledgments Financial support for this work has been provided in part by the U.S. National Science Foundation under grants EAR-0105387 and EAR-0710860 to FJS. DVW was also supported by a first-year Graduate Fellowship from Princeton University. Our Princeton colleagues Tony Dahlen (1942–2007), Jeremy Goodman (Astrophysical Sciences) and Eugene Brevdo (Electrical Engineering) each provided a key insight that helped shape the manuscript. We thank Laura Larsen-Strecker for help with the identification of geologic provinces, and Ignace Loris, Volker Michel and Mark Wieczorek for discussions. The comments by the editor, Willi Freeden, and two anonymous reviewers were all much appreciated and helped improve the manuscript. All computer code is posted on http://www.frederik.net.

References

Abramowitz, M., Stegun, I.A.: Handbook of Mathematical Functions. Dover, New York (1965)

Albertella, A., Sacerdote, F.: Using Slepian functions for local geodetic computations. Boll. Geod. Sci. Aff. **60**(1), 1–14 (2001)

Albertella, A., Sansò, F., Sneeuw, N.: Band-limited functions on a bounded spherical domain: the Slepian problem on the sphere. J. Geod. **73**, 436–447 (1999)

Amirbekyan, A., Michel, V., Simons, F.J.: Parameterizing surface-wave tomographic models with harmonic spherical splines. Geophys. J. Int. **174**(2), 617 (2008). doi:10.1111/j.1365-246X.2008.03809.x

Aronszajn, N.: Theory of reproducing kernels. Trans. Am. Math. Soc. **68**(3), 337–404 (1950)

Audet, P., Mareschal, J.-C.: Wavelet analysis of the coherence between Bouguer gravity and topography: application to the elastic thickness anisotropy in the Canadian Shield. Geophys. J. Int. **168**, 287–298 (2007). doi:10.1111/j.1365-246X.2006.03231.x

Bell, B., Percival, D.B., Walden, A.T.: Calculating Thomson's spectral multitapers by inverse iteration. J. Comput. Graph. Stat. **2**(1), 119–130 (1993)

Bertero, M., De Mol, C., Pike, E.R.: Linear inverse problems with discrete data. I. General formulation and singular system analysis. Inverse Probl. **1**, 301–330 (1985a). doi:10.1088/0266-5611/1/4/004

Bertero, M., De Mol, C., Pike, E.R.: Linear inverse problems with discrete data. II. Stability and regularisation. Inverse Probl. **1**, 301–330 (1985b). doi:10.1088/0266-5611/1/4/004

Beylkin, G., Monzón, L.: On generalized Gaussian quadratures for exponentials and their applications. Appl. Comput. Harmon. Anal. **12**, 332–372 (2002). doi:10.1006/acha.2002.0380

Beylkin, G., Sandberg, K.: Wave propagation using bases for bandlimited functions. Wave Motion **41**(3), 263–291 (2005)

Borcea, L., Papanicolaou, G., Vasquez, F.G.: Edge illumination and imaging of extended reflectors. SIAM J. Imaging Sci. **1**(1), 75–114 (2008). doi:10.1137/07069290X

Bouwkamp, C.J.: On spheroidal wave functions of order zero. J. Math. Phys. **26**, 79–92 (1947)

Boyd, J.P.: Approximation of an analytic function on a finite real interval by a bandlimited function and conjectures on properties of prolate spheroidal functions. Appl. Comput. Harmon. Anal. **15**(2), 168–176 (2003)

Boyd, J.P.: Prolate spheroidal wavefunctions as an alternative to Chebyshev and Legendre polynomials for spectral element and pseudospectral algorithms. J. Comput. Phys. **199**(2), 688–716 (2004)

Brander, O., DeFacio, B.: A generalisation of Slepian's solution for the singular value decomposition of filtered Fourier transforms. Inverse Probl. **2**, L9–L14 (1986)

Bronez, T.P.: Spectral estimation of irregularly sampled multidimensional processes by generalized prolate spheroidal sequences. IEEE Trans. Acoust. Speech Signal Process. **36**(12), 1862–1873 (1988)

Chambodut, A., Panet, I., Mandea, M., Diament, M., Holschneider, M., Jamet, O.: Wavelet frames: an alternative to spherical harmonic representation of potential fields. Geophys. J. Int. **163**(3), 875–899 (2005)

Chen, Q.Y., Gottlieb, D., Hesthaven, J.S.: Spectral methods based on prolate spheroidal wave functions for hyperbolic PDEs. Wave Motion **43**(5), 1912–1933 (2005)

Coifman, R.R., Lafon, S.: Geometric harmonics: a novel tool for multiscale out-of-sample extension of empirical functions. Appl. Comput. Harmon. Anal. **21**, 31–52 (2006). doi:10.1016/j.acha.2005.07.005

Dahlen, F.A., Simons, F.J.: Spectral estimation on a sphere in geophysics and cosmology. Geophys. J. Int. **174**, 774–807 (2008). doi:10.1111/j.1365-246X.2008.03854.x

Dahlen, F.A., Tromp, J.: Theoretical Global Seismology. Princeton University Press, Princeton, NJ (1998)

Daubechies, I.: Time–frequency localization operators: a geometric phase space approach. IEEE Trans. Inform. Theory **34**, 605–612 (1988)

Daubechies, I.: Ten Lectures on Wavelets, vol. 61 of CBMS-NSF Regional Conference Series in Applied Mathematics. Society for Industrial & Applied Mathematics, Philadelphia, PA (1992)

Daubechies, I., Paul, T.: Time–frequency localisation operators—a geometric phase space approach. II. The use of dilations. Inverse Probl. **4**(3), 661–680 (1988)

de Villiers, G.D., Marchaud, F.B.T., Pike, E.R.: Generalized Gaussian quadrature applied to an inverse problem in antenna theory. Inverse Probl. **17**, 1163–1179 (2001)

de Villiers, G.D., Marchaud, F.B.T., Pike, E.R.: Generalized Gaussian quadrature applied to an inverse problem in antenna theory: II. The two-dimensional case with circular symmetry. Inverse Probl. **19**, 755–778 (2003)

Delsarte, P., Janssen, A.J.E.M., Vries, L.B.: Discrete prolate spheroidal wave functions and interpolation. SIAM J. Appl. Math. **45**(4), 641–650 (1985)

Donoho, D.L., Stark, P.B.: Uncertainty principles and signal recovery. SIAM J. Appl. Math. **49**(3), 906–931 (1989)

Edmonds, A.R.: Angular Momentum in Quantum Mechanics. Princeton University Press, Princeton, NJ (1996)

Evans, A.J., Andrews-Hanna, J.C., Zuber, M.T.: Geophysical limitations on the erosion history within Arabia Terra. J. Geophys. Res. **115**, E05007 (2010). doi:10.1029/2009JE003469

Faÿ, G., Guilloux, F., Betoule, M., Cardoso, J.-F., Delabrouille, J., Jeune, M.L.: CMB power spectrum estimation using wavelets. Phys. Rev. D **78**, 083013 (2008). doi:10.1103/PhysRevD.78.083013

Fengler, M.J., Freeden, W., Kohlhaas, A., Michel, V., Peters, T.: Wavelet modeling of regional and temporal variations of the earth's gravitational potential observed by GRACE. J. Geod. **81**(1), 5–15 (2007). doi:10.1007/s00190-006-0040-1

Flandrin, P.: Temps-Fréquence, 2nd edn. Hermès, Paris (1998)

Freeden, W., Michel, V.: Constructive approximation and numerical methods in geodetic research today—an attempt at a categorization based on an uncertainty principle. J. Geod. **73**(9), 452–465 (1999)

Freeden, W., Windheuser, U.: Combined spherical harmonic and wavelet expansion—a future concept in Earth's gravitational determination. Appl. Comput. Harmon. Anal. **4**, 1–37 (1997)

Freeden, W., Gervens, T., Schreiner, M.: Constructive Approximation on the Sphere. Clarendon Press, Oxford (1998)

Golub, G.H., van Loan, C.F.: Matrix Computations, 2nd edn. Johns Hopkins University Press, Baltimore, MD (1989)

Gradshteyn, I.S., Ryzhik, I.M.: Tables of Integrals, Series, and Products, 6th edn. Academic Press, San Diego, CA (2000)

Grünbaum, F.A.: Eigenvectors of a Toeplitz matrix: discrete version of the prolate spheroidal wave functions. SIAM J. Algebraic Discrete Methods **2**(2), 136–141 (1981)

Grünbaum, F.A., Longhi, L., Perlstadt, M.: Differential operators commuting with finite convolution integral operators: some non-Abelian examples. SIAM J. Appl. Math. **42**(5), 941–955 (1982)

Hall, B.C., Mitchell, J.J.: Coherent states on spheres. J. Math. Phys. **43**(3), 1211–1236 (2002)

Han, S.-C.: Improved regional gravity fields on the Moon from Lunar Prospector tracking data by means of localized spherical harmonic functions. J. Geophys. Res. **113**, E11012 (2008). doi:10.1029/2008JE003166

Han, S.-C., Ditmar, P.: Localized spectral analysis of global satellite gravity fields for recovering time-variable mass redistributions. J. Geod. **82**(7), 423–430 (2007). doi:10.1007/s00190-007-0194-5

Han, S.-C., Simons, F.J.: Spatiospectral localization of global geopotential fields from the Gravity Recovery and Climate Experiment GRACE reveals the coseismic gravity change owing to the 2004 Sumatra-Andaman earthquake. J. Geophys. Res. **113**, B01405 (2008). doi:10.1029/2007JB004927

Han, S.-C., Rowlands, D.D., Luthcke, S.B., Lemoine, F.G.: Localized analysis of satellite tracking data for studying time-variable Earth's gravity fields. J. Geophys. Res. **113**, B06401 (2008a). doi:10.1029/2007JB005218

Han, S.-C., Sauber, J., Luthcke, S.B., Ji, C., Pollitz, F.F.: Implications of postseismic gravity change following the great 2004 Sumatra-Andaman earthquake from the regional harmonic analysis of GRACE inter-satellite tracking data. J. Geophys. Res. **113**, B11413 (2008b). doi:10.1029/2008JB005705

Han, S.-C., Mazarico, E., Lemoine, F.G.: Improved nearside gravity field of the Moon by localizing the power law constraint. Geophys. Res. Lett. **36**, L11203 (2009). doi:10.1029/2009GL038556

Hanssen, A.: Multidimensional multitaper spectral estimation. Signal Process. **58**, 327–332 (1997)

Harig, C., Zhong, S., Simons, F.J.: Constraints on upper-mantle viscosity inferred from the flow-induced pressure gradient across a continental keel. Geochem. Geophys. Geosyst. **11**(6), Q06004 (2010). doi:10.1029/2010GC003038

Holschneider, M., Chambodut, A., Mandea, M.: From global to regional analysis of the magnetic field on the sphere using wavelet frames. Phys. Earth Planet. Interiors **135**, 107–124 (2003)

Jackson, J.I., Meyer, C.H., Nishimura, D.G., Macovski, A.: Selection of a convolution function for Fourier inversion using gridding. IEEE Trans. Med. Imaging **10**(3), 473–478 (1991)

Jeffreys, H., Jeffreys, B.S.: Methods of Mathematical Physics, 3rd edn. Cambridge University Press, Cambridge (1988)

Karoui, A., Moumni, T.: New efficient methods of computing the prolate spheroidal wave functions and their corresponding eigenvalues. Appl. Comput. Harmon. Anal. **24**(3), 269–289 (2008)

Kennedy, R.A., Zhang, W., Abhayapala, T.D.: Spherical harmonic analysis and model-limited extrapolation on the sphere: integral equation formulation. In: Proceedings of the IEEE International Conference on Signal Processing and Communication Systems, pp. 1–6. IEEE (2008). doi:10.1109/ICSPCS.2008.4813702

Khare, K., George, N.: Sampling theory approach to prolate spheroidal wavefunctions. J. Phys. A Math. Gen. **36**, 10011–10021 (2003)

Kido, M., Yuen, D.A., Vincent, A.P.: Continuous wavelet-like filter for a spherical surface and its application to localized admittance function on Mars. Phys. Earth Planet. Interiors **135**, 1–14 (2003)

Kirby, J.F., Swain, C.J.: Mapping the mechanical anisotropy of the lithosphere using a 2D wavelet coherence, and its application to Australia. Phys. Earth Planet. Interiors **158**(2–4), 122–138 (2006). doi:10.1016/j.pepi.2006.03.022

Kowalski, K., Rembieliński, J.: Quantum mechanics on a sphere and coherent states. J. Phys. A Math. Gen. **33**, 6035–6048 (2000)

Lai, M.J., Shum, C.K., Baramidze, V., Wenston, P.: Triangulated spherical splines for geopotential reconstruction. J. Geod. **83**, 695–708 (2009). doi:10.1007/s00190-008-0283-0

Landau, H.J.: On the eigenvalue behavior of certain convolution equations. Trans. Am. Math. Soc. **115**, 242–256 (1965)

Landau, H.J., Pollak, H.O.: Prolate spheroidal wave functions, Fourier analysis and uncertainty—II. Bell Syst. Tech. J. **40**(1), 65–84 (1961)

Landau, H.J., Pollak, H.O.: Prolate spheroidal wave functions, Fourier analysis and uncertainty—III. The dimension of the space of essentially time- and band-limited signals. Bell Syst. Tech. J. **41**(4), 1295–1336 (1962)

Lilly, J.M., Park, J.: Multiwavelet spectral and polarization analyses of seismic records. Geophys. J. Int. **122**, 1001–1021 (1995)

Lindquist, M.A., Zhang, C.H., Glover, G., Shepp, L., Yang, Q.X.: A generalization of the two-dimensional prolate spheroidal wave function method for nonrectilinear MRI data acquisition methods. IEEE Trans. Image Process. **15**(9), 2792–2804 (2006). doi:10.1109/TIP.2006.877314

Liu, T.-C., van Veen, B.D.: Multiple window based minimum variance spectrum estimation for multidimensional random fields. IEEE Trans. Signal Process. **40**(3), 578–589 (1992). doi:10.1109/78.120801

Ma, J., Rokhlin, V., Wandzura, S.: Generalized Gaussian quadrature rules for systems of arbitrary functions. SIAM J. Numer. Anal. **33**(3), 971–996 (1996)

Mallat, S.: A Wavelet Tour of Signal Processing. Academic Press, San Diego, CA (1998)

Maniar, H., Mitra, P.P.: The concentration problem for vector fields. Int. J. Bioelectromagn. **7**(1), 142–145 (2005)

Marinucci, D., Pietrobon, D., Balbi, A., Baldi, P., Cabella, P., Kerkyacharian, G., Natoli, P., Picard, D., Vittorio, N.: Spherical needlets for cosmic microwave background data analysis. Monthly Notices R. Astron. Soc. **383**(2), 539–545 (2008). doi:10.1111/j.1365-2966.2007.12550.x

McEwen, J.D., Hobson, M.P., Mortlock, D.J., Lasenby, A.N.: Fast directional continuous spherical wavelet transform algorithms. IEEE Trans. Signal Process. **55**(2), 520–529 (2007)

Michel, V., Wolf, K.: Numerical aspects of a spline-based multiresolution recovery of the harmonic mass density out of gravity functionals. Geophys. J. Int. **173**, 1–16 (2008). doi:10.1111/j.1365-246X.2007.03700.x

Miranian, L.: Slepian functions on the sphere, generalized Gaussian quadrature rule. Inverse Probl. **20**, 877–892 (2004)

Mitra, P.P., Maniar, H.: Concentration maximization and local basis expansions (LBEX) for linear inverse problems. IEEE Trans. Biomed Eng. **53**(9), 1775–1782 (2006)

Moore, I.C., Cada, M.: Prolate spheroidal wave functions, an introduction to the Slepian series and its properties. Appl. Comput. Harmon. Anal. **16**, 208–230 (2004)

Narcowich, F.J., Ward, J.D.: Nonstationary wavelets on the m-sphere for scattered data. Appl. Comput. Harmon. Anal. **3**, 324–336 (1996)

Nashed, M.Z., Walter, G.G.: General sampling theorems for functions in Reproducing Kernel Hilbert Spaces. Math. Control Signals Syst. **4**, 363–390 (1991)

Nyström, E.J.: Über die praktische Auflösung von Integralgleichungen mit Anwendungen auf Randwertaufgaben. Acta Math. **54**, 185–204 (1930)

Olhede, S., Walden, A.T.: Generalized Morse wavelets. IEEE Trans. Signal Process. **50**(11), 2661–2670 (2002)

Olhede, S.C., Metikas, G.: The monogenic wavelet transform. IEEE Trans. Signal Process. **57**(9), 3426–3441 (2009). doi:10.1109/TSP.2009.2023397

Panet, I., Chambodut, A., Diament, M., Holschneider, M., Jamet, O.: New insights on intraplate volcanism in French Polynesia from wavelet analysis of GRACE, CHAMP, and sea surface data. J. Geophys. Res. **111**, B09403 (2006). doi:10.1029/2005JB004141

Papoulis, A.: A new algorithm in spectral analysis and band-limited extrapolation. IEEE-CS **22**(9), 735–742 (1975)

Parks, T.W., Shenoy, R.G.: Time–frequency concentrated basis functions. In: Proceedings of the IEEE International Conference on Acoustics, Speech, and Signal Processing, vol. 5, pp. 2459–2462. IEEE (1990)

Parlett, B.N., Wu, W.-D.: Eigenvector matrices of symmetric tridiagonals. Numer. Math. **44**, 103–110 (1984)

Percival, D.B., Walden, A.T.: Spectral Analysis for Physical Applications, Multitaper and Conventional Univariate Techniques. Cambridge University Press, New York (1993)

Percival, D.B., Walden, A.T.: Wavelet Methods for Time Series Analysis. Cambridge University Press, Cambridge (2006)

Press, W.H., Teukolsky, S.A., Vetterling, W.T., Flannery, B.P.: Numerical Recipes in FORTRAN: The Art of Scientific Computing, 2nd edn. Cambridge University Press, New York (1992)

Ramesh, P.S., Lean, M.H.: Accurate integration of singular kernels in boundary integral formulations for Helmholtz equation. Int. J. Numer. Methods Eng. **31**, 1055–1068 (1991)

Riedel, K.S., Sidorenko, A.: Minimum bias multiple taper spectral estimation. IEEE Trans. Signal Process. **43**(1), 188–195 (1995)

Saito, N.: Data analysis and representation on a general domain using eigenfunctions of Laplacian. Appl. Comput. Harmon. Anal. **25**, 68–97 (2007). doi:10.1016/j.acha.2007.09.005

Schmidt, M., Han, S.-C., Kusche, J., Sanchez, L., Shum, C.K.: Regional high-resolution spatiotemporal gravity modeling from GRACE data using spherical wavelets. Geophys. Res. Lett. **33**(8), L0840 (2006). doi:10.1029/2005GL025509

Schmidt, M., Fengler, M., Mayer-Gürr, T., Eicker, A., Kusche, J., Sánchez, L., Han, S.-C.: Regional gravity modeling in terms of spherical base functions. J. Geod. **81**(1), 17–38 (2007). doi:10.1007/s00190-006-0101-5

Schott, J.-J., Thébault, E.: Modelling the Earths magnetic field from global to regional scales. In: Mandea, M., Korte, M. (eds.) Geomagnetic Observations and Models, vol. 5 of IAGA Special Sopron Book Series. Springer, Berlin (2011)

Shepp, L., Zhang, C.-H.: Fast functional magnetic resonance imaging via prolate wavelets. Appl. Comput. Harmon. Anal. **9**(2), 99–119 (2000). doi:10.1006/acha.2000.0302

Shkolnisky, Y.: Prolate spheroidal wave functions on a disc—integration and approximation of two-dimensional bandlimited functions. Appl. Comput. Harmon. Anal. **22**, 235–256 (2007). doi:10.1016/j.acha.2006.07.002

Shkolnisky, Y., Tygert, M., Rokhlin, V.: Approximation of bandlimited functions. Appl. Comput. Harmon. Anal. **21**, 413–420 (2006). doi:10.1016/j.acha.2006.05.001

Simons, F.J.: Slepian functions and their use in signal estimation and spectral analysis. In: Freeden, W., Nashed, M.Z., Sonar, T. (eds.) Handbook of Geomathematics, chap. 30, pp. 891–923. Springer, Heidelberg (2010). doi:10.1007/978-3-642-01546-5_30

Simons, F.J., Dahlen, F.A.: Spherical Slepian functions and the polar gap in geodesy. Geophys. J. Int. **166**, 1039–1061 (2006). doi:10.1111/j.1365-246X.2006.03065.x

Simons, F.J., Dahlen, F.A.: A spatiospectral localization approach to estimating potential fields on the surface of a sphere from noisy, incomplete data taken at satellite altitudes. In: Van de Ville, D., Goyal, V.K., Papadakis, M. (eds.) Wavelets XII, vol. 6701, p. 670117. SPIE (2007). doi:10.1117/12.732406

Simons, F.J., van der Hilst, R.D., Zuber, M.T.: Spatio-spectral localization of isostatic coherence anisotropy in Australia and its relation to seismic anisotropy: Implications for lithospheric deformation. J. Geophys. Res. **108**(B5) 2250. doi:10.1029/2001JB000704

Simons, F.J., Dahlen, F.A., Wieczorek, M.A.: Spatiospectral concentration on a sphere. SIAM Rev. **48**(3), 504–536 (2006). doi:10.1137/S0036144504445765

Simons, F.J., Hawthorne, J.C., Beggan, C.D.: Efficient analysis and representation of geophysical processes using localized spherical basis functions. In: Goyal, V.K., Papadakis, M., Van de Ville, D. (eds.) Wavelets XIII, vol. 7446, p. 74460G. SPIE (2009). doi:10.1117/12.825730

Simons, M., Solomon, S.C., Hager, B.H.: Localization of gravity and topography: constraints on the tectonics and mantle dynamics of Venus. Geophys. J. Int. **131**, 24–44 (1997)

Slepian, D.: Prolate spheroidal wave functions, Fourier analysis and uncertainty—IV. Extensions to many dimensions; generalized prolate spheroidal functions. Bell Syst. Tech. J. **43**(6), 3009–3057 (1964)

Slepian, D.: On bandwidth. Proc. IEEE **64**(3), 292–300 (1976)

Slepian, D.: Prolate spheroidal wave functions, Fourier analysis and uncertainty—V. The discrete case. Bell Syst. Tech. J. **57**, 1371–1429 (1978)

Slepian, D.: Some comments on Fourier analysis, uncertainty and modeling. SIAM Rev. **25**(3), 379–393 (1983)

Slepian, D., Pollak, H.O.: Prolate spheroidal wave functions, Fourier analysis and uncertainty—I. Bell Syst. Tech. J. **40**(1), 43–63 (1961)

Slepian, D., Sonnenblick, E.: Eigenvalues associated with prolate spheroidal wave functions of zero order. Bell Syst. Tech. J. **44**(8), 1745–1759 (1965)

Tegmark, M.: A method for extracting maximum resolution power spectra from galaxy surveys. Astrophys. J. **455**, 429–438 (1995)

Tegmark, M.: A method for extracting maximum resolution power spectra from microwave sky maps. Monthly Notices R. Astron. Soc. **280**, 299–308 (1996)

Thomson, D.J.: Spectrum estimation and harmonic analysis. Proc. IEEE **70**(9), 1055–1096 (1982)

Thomson, D.J.: Quadratic-inverse spectrum estimates: applications to paleoclimatology. Phil. Trans. R. Soc. Lond. Ser. A **332**(1627), 539–597 (1990)

Tricomi, F.G.: Integral Equations, 5th edn. Interscience, New York (1970)

Van De Ville, D., Unser, M.: Complex wavelet bases, steerability, and the Marr-like pyramid. IEEE Trans. Image Process. **17**(11), 2063–2080 (2008). doi:10.1109/TIP.2008.2004797

Van De Ville, D., Philips, W., Lemahieu, I.: On the N-dimensional extension of the discrete prolate spheroidal window. IEEE Trans. Signal Process. **9**(3), 89–91 (2002)

Walden, A.T.: Improved low-frequency decay estimation using the multitaper spectral-analysis method. Geophys. Prospect. **38**, 61–86 (1990)
Walter, G., Soleski, T.: A new friendly method of computing prolate spheroidal wave functions and wavelets. Appl. Comput. Harmon. Anal. **19**, 432–443 (2005)
Walter, G.G., Shen, X.: Wavelets based on prolate spheroidal wave functions. J. Fourier Anal. Appl. **10**(1), 1–26 (2004). doi:10.1007/s00041-004-8001-7
Walter, G.G., Shen, X.: Wavelet like behavior of Slepian functions and their use in density estimation. Commun. Stat. Theory Methods **34**(3), 687–711 (2005)
Walter, G.G., Soleski, T.: Error estimates for the PSWF method in MRI. Contemp. Math. **451**, 262 (2008)
Wei, L., Kennedy, R.A., Lamahewa, T.A.: Signal concentration on unit sphere: an azimuthally moment weighting approach. In: Proceedings of the IEEE International Conference on Acoustics, Speech, and Signal Processing, pp. 1–4. IEEE (2010)
Wieczorek, M.A., Simons, F.J.: Localized spectral analysis on the sphere. Geophys. J. Int. **162**(3), 655–675 (2005). doi:10.1111/j.1365-246X.2005.02687.x
Wieczorek, M.A., Simons, F.J.: Minimum-variance spectral analysis on the sphere. J. Fourier Anal. Appl. **13**(6), 665–692 (2007). doi:10.1007/s00041-006-6904-1
Wingham, D.J.: The reconstruction of a band-limited function and its Fourier transform from a finite number of samples at arbitrary locations by Singular Value Decomposition. IEEE Trans. Signal Process. **40**(3), 559–570 (1992). doi:10.1109/78.120799
Xiao, H., Rokhlin, V., Yarvin, N.: Prolate spheroidal wavefunctions, quadrature and interpolation. Inverse Probl. **17**, 805–838 (2001). doi:10.1088/0266-5611/17/4/315
Yang, Q.X., Lindquist, M.A., Shepp, L., Zhang, C.-H., Wang, J., Smith, M.B.: Two dimensional prolate spheroidal wave functions for MRI. J. Magn. Reson. **158**, 43–51 (2002)
Yao, K.: Application of reproducing kernel Hilbert spaces—bandlimited signal models. Inf. Control **11**(4), 429–444 (1967)
Zhang, X.: Wavenumber spectrum of very short wind waves: an application of two-dimensional Slepian windows to spectral estimation. J. Atmos. Ocean. Technol. **11**, 489–505 (1994)
Zhou, Y., Rushforth, C.K., Frost, R.L.: Singular value decomposition, singular vectors, and the discrete prolate spheroidal sequences. Proc. IEEE Int. Conf. Acoust. Speech Signal Process. **9**(1), 92–95 (1984)